Similarity of Microclimate as Simulated in Response to Landscapes of the 1930s and the 1980s

NICOLE MÖLDERS

Institut für Meteorologie, Universität Leipzig, Leipzig, Germany

(Manuscript received 30 September 1999, in final form 29 March 2000)

ABSTRACT

In the time between the 1930s and the 1980s land use was modified by deforestation, urbanization, afforestation and recultivation of open-pit mines, further installation of open-pit mines, and drainage in about 46% of a 30 000 km^2 area in the south Brandenburg/north Saxony region of Germany (51°00′N, 11°58′E; 52°17′N, 11°53′E; 51°00′N, 14°54′E; 52°17′N, 14°49′E). This study evaluates the short-term (1 day) impacts of these land use changes assuming the same typical day in May for both landscapes. In so doing, a state-of-the-art, meso-β-scale atmospheric model is applied with a resolution of 5 km × 5 km on the coarse grid and 1 km × 1 km on the subgrid.

Under the land use of the 1980s, the simulated atmospheric boundary layer (ABL) is slightly warmer and drier than it was in the 1930s. The sensitivity of the ABL to the changes in land use varies with time. The calculated probability density functions show that the partitioning of incoming energy between sensible and latent heat and the partitioning of cloud microphysical processes between the warm and cold paths of precipitation formation differ appreciably. The cloud and precipitation distributions are affected the most of all the variables examined here. For precipitation, simply changing coniferous forest to its full extent in the 1980s may provide results even more dissimilar when compared with results provided by a 1930s landscape than does a simulation with a 1980s landscape.

Deviations from the principle of superposition of the responses of the simple land use changes can be induced by primary (land use changes) and secondary (e.g., altered cloud distributions as a response to the land use modifications) differences. Diminution or enhancement of the atmospheric response depends on 1) the size of the resulting new patch as well as the uniformity of its land use, 2) the kind of change in the hydrologic and thermal characteristics, and 3) the type of land use prevailing in the environments of land use conversion. According to the results of this case study, areas dominated by grassland and forests are more sensitive to concurrent land use changes than are prevailingly agriculturally used areas.

1. Introduction

In recent years there has been a heightened awareness in the general public of climate changes, especially those changes that are anthropogenically induced. An altered climate is the response to a number of relevant climatic aspects such as astronomical, geophysical, chemical, and biospheric conditions as well as anthropogenic influences such as the emission of trace gases or changes in land use. Out of the variety of possible anthropogenic influences on climate, land use conversions brought on by subsidization policies, urbanization, deforestation, and afforestation seem to be of special interest for many policy areas, not the least of which are water and food resource management.

Land use changes mean a change of surface properties (e.g., albedo, roughness length, maximum evaporative conductivity, heterogeneity; see also Table 1). An increase of albedo, for instance, may decrease the surface moist static energy flux (e.g., Pan et al. 1999), and a reduction in roughness lessens vertical mixing (e.g., Mölders 1999a,b). The size of the new patches, that is, the degree of surface heterogeneity, determines whether distinct patterns of upward or downward motions may be established (e.g., Friedrich and Mölders 2000). Thus, land use changes may affect the microclimate in several ways. They may alter 1) the partitioning of incoming solar energy into sensible and latent heat fluxes (e.g., Cotton and Pielke 1995), 2) the fraction of solar radiation scattered back to space (e.g., Pan et al. 1999), 3) the structure of the atmospheric boundary layer (ABL; e.g., Pielke et al. 1991), 4) the thermodynamic environment for convection and thus moist static energy (e.g., Anthes 1984; Pan et al. 1999), 5) the dynamics (e.g., Loose and Bornstein 1977), and 6) runoff (e.g., Calder et al. 1995) by nonlinear feedback mechanisms of higher degrees of complexity.

Corresponding author address: Nicole Mölders, Institut für Meteorologie, Universität Leipzig, Stephanstraße 3, D-04103 Leipzig, Germany.
E-mail: moelders@curie.meteo.uni-leipzig.de

TABLE 1. Thermal diffusivity of the soil k_s, heat capacity c_i, emissivity ε, albedo α, roughness length z_0, field capacity weighted by the uppermost diurnally active soil layer w_k, capillarity α_c, and maximal evaporative conductivity g_1 used in the model (Pielke 1984; Wilson et al. 1986; Eppel et al. 1995). Because grassland represents short-cutted water meadows in most cases, the albedo of short grass is taken. Parameters denoted by * are calculated by the model.

Land use type	k_s (10^{-6} m^2 s^{-1})	c_i [10^6 J (m^3 K)$^{-1}$]	ε	α	z_0 (m)	w_k (m)	α_c [10^{-3} kg (m^3 s)$^{-1}$]	g_1 (m s^{-1})
Water	0.15	4.2	0.94	*	*	1.0	1000	–
Open-pit mine	0.84	2.1	0.90	0.3	0.0004	0.002	0.9	–
Marshland	0.12	3.1	0.98	0.1	0.15	0.008	6.0	0.024
Grassland	0.56	2.1	0.95	0.25	0.02	0.010	8.0	0.04
Agriculture	0.74	2.9	0.95	0.18	0.04	0.003	3.0	0.04
Heath	0.70	2.5	0.95	0.15	0.35	0.003	1.0	0.024
Deciduous forest	0.70	2.5	0.97	0.20	0.8	0.010	8.0	0.023
Mixed forest	0.70	2.5	0.975	0.175	0.9	0.010	8.0	0.023
Coniferous forest	0.70	2.5	0.98	0.15	1.0	0.010	8.0	0.023
Village	1.0	2.0	0.90	0.20	0.8	0.003	1.0	–
City	1.0	2.0	0.95	0.15	1.0	0.002	0.9	–

Several recent studies have examined the effect of altered land use at regional and global scales. For instance, Anthes (1984) found that planting bands of vegetation with width on the order of 50–100 km in semiarid regions could result in increases of convection and precipitation that could be greater than those associated with uniform vegetating of large areas. Zhang et al. (1996) showed that Amazonian deforestation affected significantly the Walker and Hadley circulations and resulted in changes distant from the region of deforestation by Rossby wave propagation mechanisms. In investigating the regional response to the desertification of the former Mongolian grassland, Xue (1996) found a weakening of the monsoon circulation and a reduction in convective latent heating. Copeland et al. (1996) examined the continent-wide land use changes caused by the settling of America. The quantitative changes of flood and drought years are opposite to those of normal years for these land use changes (Pan et al. 1999). Using the 1900, 1973, and 1993 landscapes of southern Florida, Pielke et al. (1999) found that average summer rainfall decreased by 9% for the 1973 landscape and 11% for the 1993 landscape as compared with the model results when the 1900 landscape is used. The limited available observations of trends in summer rainfall over this region are consistent with these trends. The effect of local-scale land use changes on local meteorological conditions was investigated mainly within the framework of planning (e.g., Groß 1988, 1989; Mölders 1998, 2000) or sensitivity studies (e.g., Mölders 1999a,b, 2000). Although the scales of the aforementioned studies differ, their results all indicate substantial differences in screen-height temperature, humidity, wind speed, and precipitation as the outcome of the land use changes. The big differences in the aforementioned quantities are related closely to the altered vegetation parameters. Note that Mölders (1999b) showed that the qualitative effect of land use changes on cloud and precipitation formation is independent of the cloud microphysical parameterization applied.

Recent land use changes usually take place on a local scale. Because there are various interaction and feedback processes between some of the climate-determining conditions, the knowledge of the influences of various processes and their responses to local-scale land use changes on microclimatic conditions is a prerequisite to a better understanding of climate. At the earth–atmosphere interface, the fluxes of momentum, water, and energy are regulated by the biogeophysical processes governed by surface characteristics. Consequently, one has to look at their respective temporal and spatial scales as well as at possible (nonlinear) feedback. Many land surface properties have effects that occur on scales of weeks or seasons (e.g., Copeland et al. 1996; Xue 1996; Zhang et al. 1996; Claussen 1997; Pielke et al. 1999). To understand these effects, the influence of the altered surface properties on the processes has to be examined.

Therefore, the influence of the local-scale land use changes that occurred in southern Brandenburg and northern Saxony (51°00′N, 11°58′E; 52°17′N, 11°53′E; 51°00′N, 14°54′E; 52°17′N, 14°49′E) between the 1930s and 1980s (Fig. 1) on micrometeorological (e.g., evapotranspiration) and meso-γ/β-scale processes (e.g., recycling of water within an area) is examined within their typical temporal scales of hours to a day in this study. In this area, one has seen how the increase of population, economic development, open-pit mining, drainage of marshland, recultivation of military areas, and modified agricultural practices have all contributed appreciably to alterations in the landscape (e.g., Fig. 1). Herein, as defined by Mölders (2000), *concurrent* land use changes occur, that is, different land use types A, B, C, and so on, are simultaneously converted to various land use types X, Y, Z, and so on. For the purpose of this study, simulations are performed with the nonhydrostatic meso-β-scale meteorological Geesthacht's Simulation Model of the Atmosphere (GESIMA; see Kapitza and Eppel 1992; Eppel et al. 1995). In these simulations, data are alternatively applied that represented these landscapes in the 1930s and 1980s.

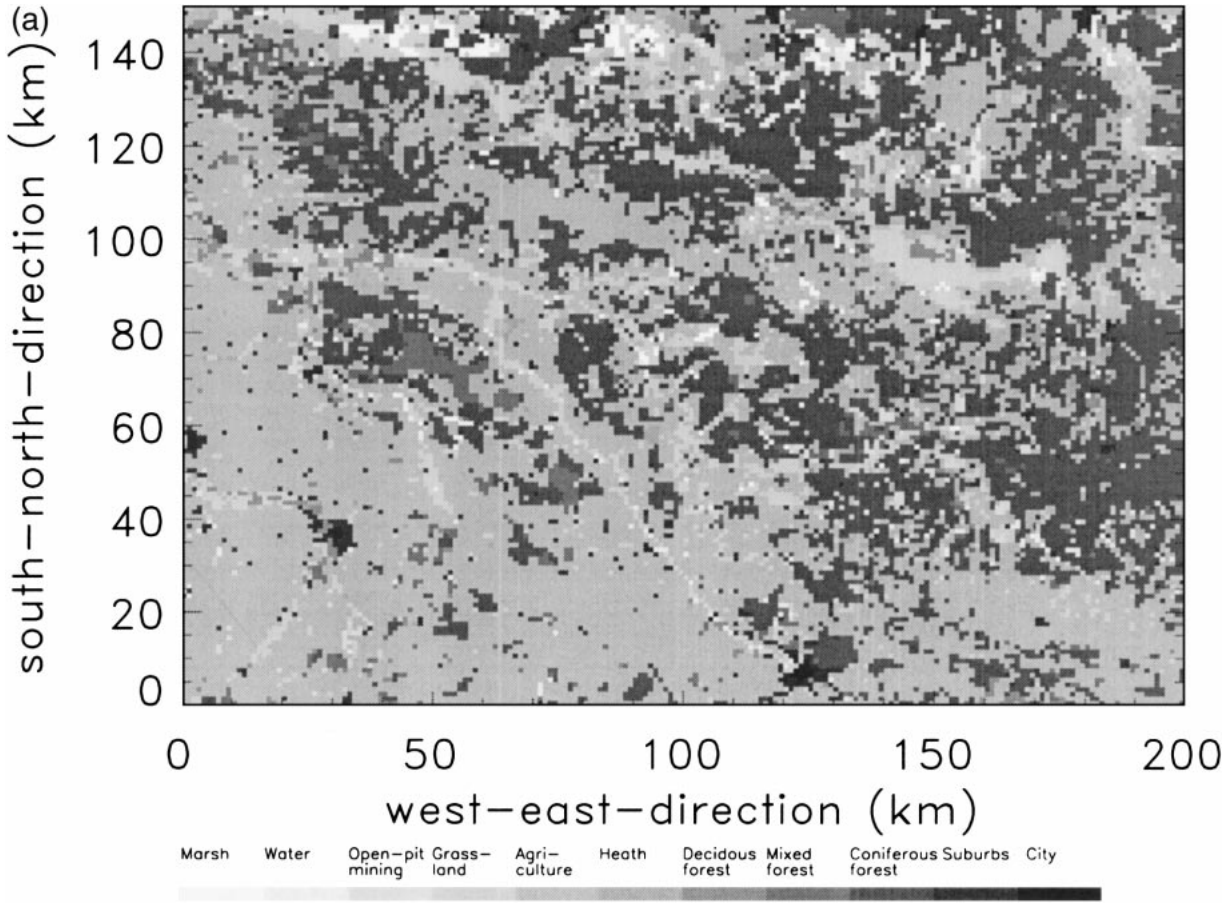

FIG. 1. Distribution of surface characteristics for (a) the 1930s and (b) the 1980s. See text for a description of the major changes. The area encompasses 30 000 km^2 of northern Saxony and southern Brandenburg (51°00′N, 11°58′E; 52°17′N, 11°53′E; 51°00′N, 14°54′E; 52°17′N, 14°49′E), which is located south of Berlin, Germany.

2. Model and data

a. Brief description of the model

The main dynamical, numerical, and physical features of GESIMA are given in Kapitza and Eppel (1992) and Eppel et al. (1995). The model physics used in this study differs from that described by Eppel et al. (1995) by 1) the inclusion of an explicit subgrid scheme to consider subgrid-scale heterogeneity of precipitation and subgrid-scale surface heterogeneity in a finer resolution than the grid resolution of the atmospheric model (e.g., Mölders et al. 1996); 2) the determination of the surface stress and near-surface fluxes of heat and water vapor by use of Kramm et al.'s (1995) parametric model, wherein these fluxes are expressed in terms of dimensionless drag coefficients and transfer coefficients of heat and moisture; 3) the treatment of cloud microphysics by a five-water-class bulk parameterization scheme that includes water vapor, cloud water, rainwater, ice, and graupel (e.g., Mölders et al. 1997a); and 4) the modification of GESIMA's land surface scheme (see Mölders 1998). More details of the model configuration as applied in this study can be found in Mölders (1998, 1999a,b, 2000).

GESIMA and its modules have been validated for a wide range of applications (e.g., Claussen 1988; Kapitza and Eppel 1992; Levkov et al. 1992; Eppel et al. 1995; Devantier and Raabe 1996; Hinneburg and Tetzlaff 1996; Mölders 1998, 1999a). Moreover, GESIMA has shown itself able to simulate atmospheric responses to surface characteristics that usually are observed (Mölders 1998).

b. Model domain, resolution, grid spacing, and boundary conditions

The inner model domain encompasses the troposphere over southern Brandenburg and northern Saxony (Fig. 1). It extends 200 km in an east–west direction and 150 km in a south–north direction. Outside of this domain, five grid points are chosen to be the same for all runs. The vertical resolution varies from 20 m near the ground to 1 km at a height of 10 km. Above and below a height of 2 km there are eight levels. The hor-

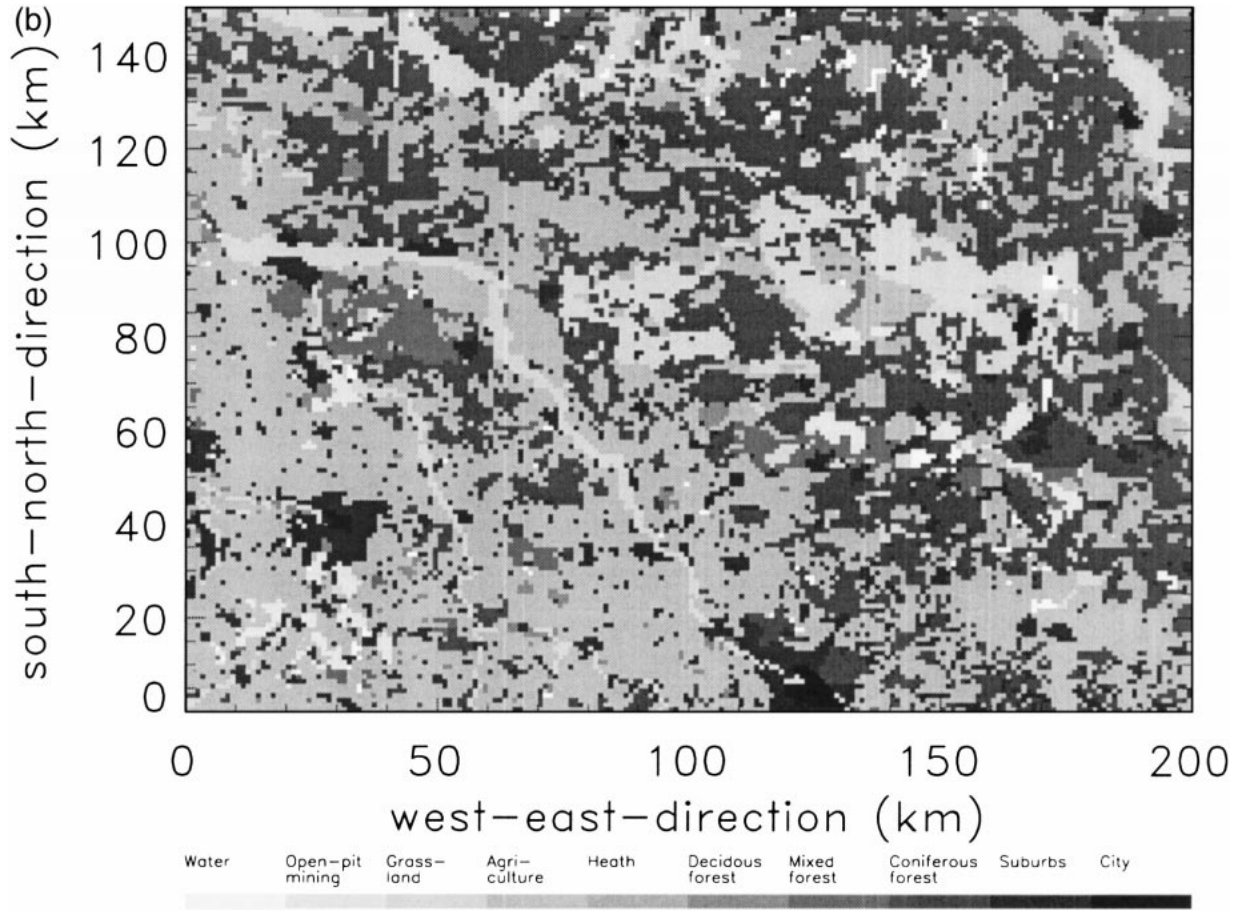

FIG. 1. (*Continued*)

izontal grid spacing is 5 km × 5 km for the atmospheric grid cells. Within the framework of the explicit subgrid scheme, each atmospheric grid cell falls into 25 subgrid cells of 1 km × 1 km each at the earth–atmosphere boundary and within the soil. The subgrid cells are assumed to be homogeneously covered by their individual vegetation over horizontally homogeneous soil types. Energy and water fluxes for each of these subgrid cells are solved by applying the soil- and plant-specific parameters (Table 1), soil forcing (i.e., ground and soil temperature, and soil wetness), and near-surface meteorological forcing of these subgrid cells (e.g., near-surface air temperature and humidity). Arithmetical averaging of the subgrid fluxes realizes the coupling of the subgrid cells to the atmospheric grid cell. Note that the subgrid scheme allows one to consider land use changes on a realistic meso-γ-scale size.

At the top of the model, a rigid lid together with a sponge layer to absorb vertically propagating gravity waves is used. At the lateral boundaries, the Orlanski (1976) radiation boundary condition is applied for the normal component of momentum, and a zero-gradient method is used for all other variables.

c. Land use data of the 1930s and the 1980s

To determine the surface characteristics of the 1930s, historic maps are digitized (see Fig. 1). These maps originate from about 1900 and were updated continually until 1939. Because of their poor graphic quality there may be errors from the digitizing procedure. The latest recently updated maps originate from the late 1980s (1986–89). Although more recent data are available from satellite (e.g., Mölders et al. 1997b), the aforementioned maps were digitized to ensure the same method for deriving data for the 1930s and 1980s. Note that alternatively applying digitized and satellite-derived land use data may lead to appreciable differences in the daily averages of simulated soil moisture, surface temperature, and sensible and latent heat fluxes, although the distribution of daily averages of simulated temperature and humidity differ only slightly (Mölders et al. 1997b). Hereinafter, the land use data of the 1930s and 1980s are denoted S30 and S80, respectively, as are the simulations performed with these datasets and their results.

In the northeastern part of the domain, forest and

TABLE 2. Percentage of the domain (30 000 km^2) that is of land use type A in S30 (columns) and of land use type B in S80 (rows). Note that neither marshland nor heath exists on the resolution of the digitization (1 km $\times$ 1 km) in S80. The value listed for equal land use types in S30 and S80 represents the percentage of unchanged area covered by said land use. The columns and rows add up to the percentage of the various land use types in S30 and S80 (total), respectively.

Land use	Marshland	Water	Open-pit mine	Grassland	Agriculture	Heath	Deciduous forest	Mixed forest	Coniferous forest	Village	City	Total S80
Water	0.02	0.18	0.02	0.05	0.24	0.00	0.00	0.03	0.29	0.03	0.00	0.86
Open-pit mine	0.00	0.01	0.01	0.11	0.68	0.01	0.01	0.07	0.46	0.04	0.00	1.40
Grassland	0.38	0.19	0.07	3.73	4.00	0.20	0.29	0.15	1.67	0.16	0.01	10.85
Agriculture	0.22	0.25	0.18	3.33	30.62	0.37	0.33	0.83	7.52	0.65	0.01	44.31
Deciduous forest	0.00	0.00	0.00	0.10	0.44	0.01	0.11	0.03	0.24	0.03	0.00	0.96
Mixed forest	0.04	0.02	0.06	0.33	0.84	0.03	0.07	0.33	1.46	0.06	0.00	3.24
Coniferous forest	0.36	0.30	0.20	1.73	7.12	0.31	0.22	1.40	18.23	0.37	0.00	30.24
Village	0.03	0.10	0.08	0.65	4.50	0.05	0.13	0.16	1.14	0.74	0.11	7.69
City	0.00	0.01	0.00	0.03	0.17	0.01	0.01	0.00	0.05	0.11	0.06	0.45
Total S30	1.05	1.06	0.62	10.06	48.61	0.99	1.17	3.00	31.06	2.19	0.19	

TABLE 3. List of simulations performed in this study.

Name	Land use data	Changes
S30	Digitized from historical maps	None
S30W	Like S30 but all pixels that are water in S80 are changed to water	Simple
S30O	Like S30 but all pixels that are open-pit mine in S80 are changed to open-pit mine	Simple
S30G	Like S30 but all pixels that are grassland in S80 are changed to grassland	Simple
S30A	Like S30 but all pixels that are agriculture in S80 are changed to agriculture	Simple
S30D	Like S30 but all pixels that are deciduous forest in S80 are changed to deciduous forest	Simple
S30M	Like S30 but all pixels that are mixed forest in S80 are changed to mixed forest	Simple
S30C	Like S30 but all pixels that are coniferous forest in S80 are changed to coniferous forest	Simple
S30V	Like S30 but all pixels that are village in S80 are changed to village	Simple
S30T	Like S30 but all pixels that are city in S80 are changed to city	Simple
S80	Digitized from recent maps of the 1980s	Concurrent

grassland prevail, and, in the southwestern part, land used agriculturally dominates (Fig. 1). Open-pit mining exists in Südraum Leipzig (outskirts of Leipzig), Bitterfelder Revier (mining district of Bitterfeld), and Oberlausitz (area south of Bautzen) and Niederlausitz (Fig. 1). In the 1980s, only 54.01% of the land surface cover remained the same as in the 1930s (Table 2). Thus, these landscape changes are much greater than those resulting from urbanization and various recultivation scenarios as assumed in Mölders's (2000) ''future'' study.

In the earlier maps, settlements cover an appreciably smaller fraction of the domain, and grassland takes up an appreciably larger fraction as compared with the maps of the 1980s (Fig. 1; Table 2). The decrease in grassland coverage may be explained partly by the limited graphic quality of the earlier maps. Furthermore, in the maps of the 1980s, only water meadows are indicated as grassland. In the area between 90–100 and 20–40 km (Fig. 1; counted from the western and southern edge of the domain; note that counting will be this way throughout the discussion), largely extended water meadows exist in the 1930s but not in the 1980s. This land use change gives the impression of an altered course of the Elbe River (see also Fig. 1).

In the maps of the 1980s, deciduous and coniferous forests are seldom distinguished. As a result, mixed forest occurs more frequently in these maps than in those of the 1930s (Fig. 1, Table 2).

In the 1930s, the Elbe River still retained its natural form and took up a larger area than in the 1980s. Thus, it is sometimes dominant at the 1 km $\times$ 1 km resolution (Fig. 1). Flooding of open-pit mines or artificial water reservoirs lead to changes in water in S80.

Mining activity changed from operating many small open-pit mines, which are often of subgrid scale relative

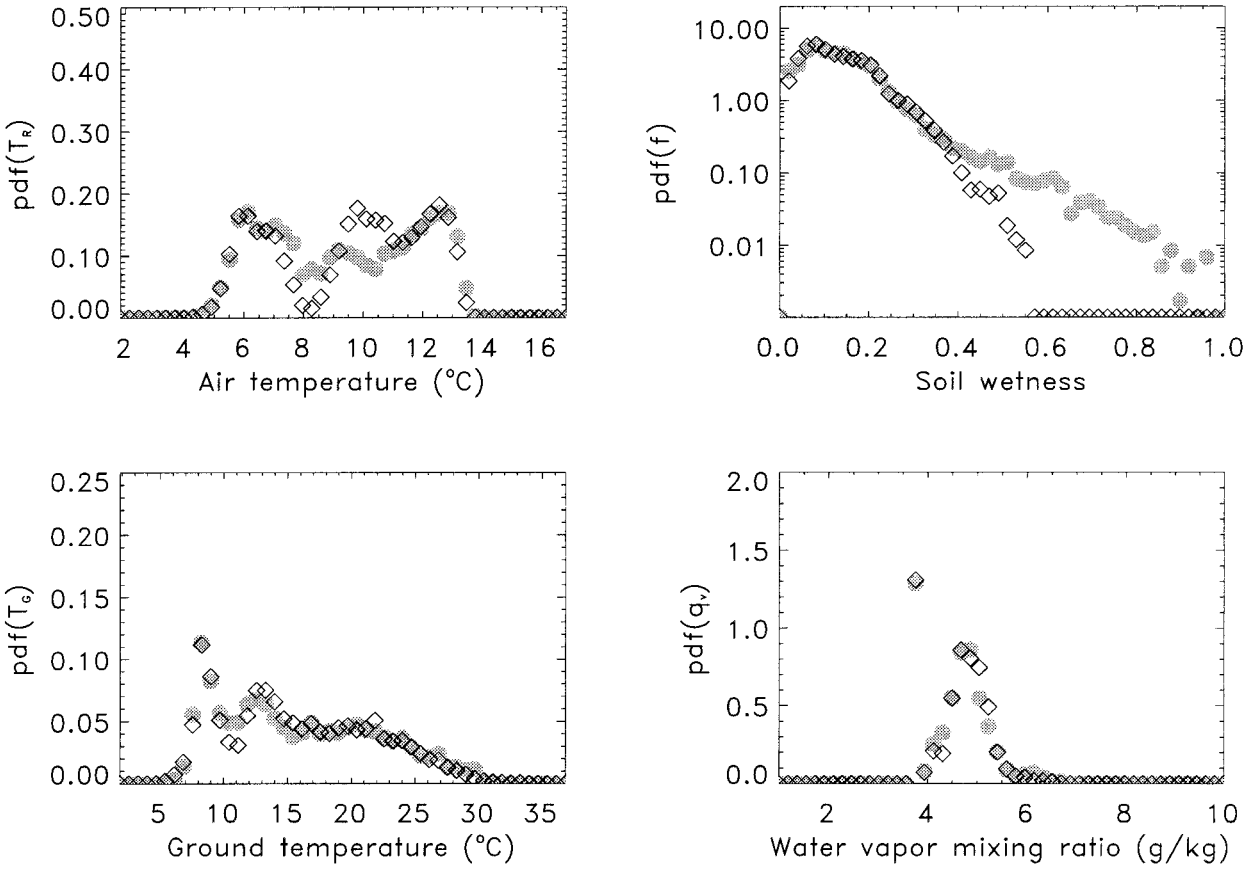

FIG. 2. Comparison of probability density functions of air temperature T_R at reference height, soil wetness factor f, ground temperature T_G, and specific humidity at reference height q_v (upper left to lower right) as determined for S30 (gray circles) and S80 (diamonds).

to the digitizing grid, to fewer but larger ones. Although in the 1930s, heath and marshland each cover about 1% of the domain (Fig. 1; e.g., at 110 km, 140 km; in the Fläming at 20 km, 130 km), they are of subgrid scale with respect to the resolution of 1 km × 1 km and thus do not occur in S80 (Fig. 1, Table 2).

d. Topography data of the 1930s and the 1980s

The historic terrain height is assumed to be equal to that of S80 except for open-pit mines (for topography of the 1980s, see Fig. 1 in Mölders 1999a). In the maps of the 1980s, terrain height before the onset of mining activities is also given for the mining areas. Thus this terrain height is taken for S30 in those areas where mining exists in the 1980s but not in the 1930s. The elevations of open-pit mines in the 1930s that already are recultivated in the 1980s are assumed to be 10 m below the average terrain height of the same 1 km × 1 km areas in S80.

e. Soil data of the 1930s and the 1980s

According to the theory developed by Eagleson (1982), in which climate, soil, and vegetation evolve synergistically, soil type is coupled to land use type for simplicity (e.g., Eppel et al. 1995; Mölders 1998, 1999a,b, 2000). Most of the land use conversions (e.g., to open-pit mine or to settlements) occurring between the 1930s and the 1980s are accompanied by appreciable changes in soil and surface characteristics. In Brandenburg and northern Saxony, for instance, converting grassland or marshland to agriculturally used land means that draining had to be performed. Thus for simplicity's sake, in this study, soil type changes with land use type (Table 1). This approach means that, if the land use changes from grassland to open-pit mine or from agriculture to village, the soil characteristics (capillarity, field capacity, thermal diffusivity, and heat capacity) are altered in accordance with Table 1.

3. Design of the study

a. Initialization of the simulations

In nature, land use changes could possibly affect the profiles in the ABL. Moreover, the large-scale climate of the 1930s and 1980s differs slightly. For comparison and to avoid additional degrees of freedom, all simulations start at each grid column with the same vertical

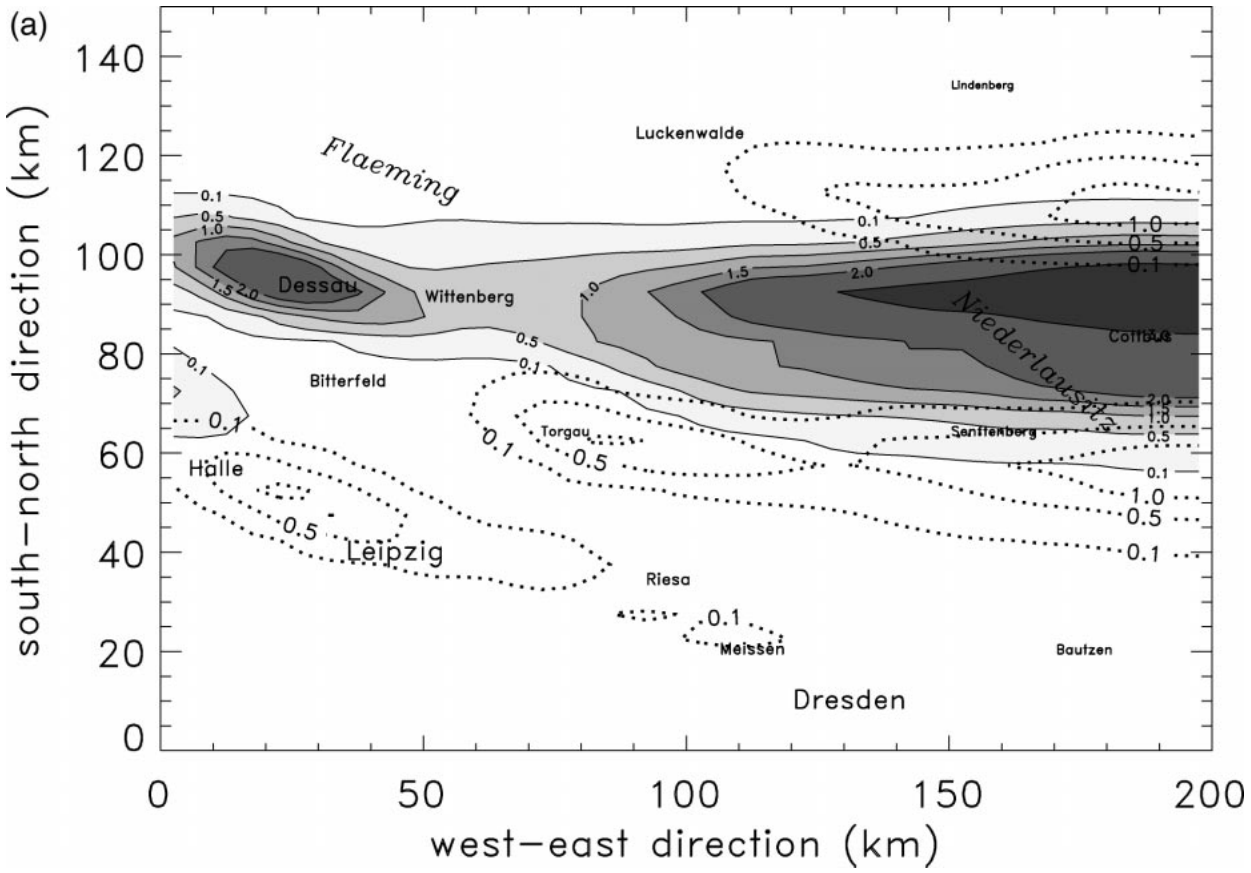

FIG. 3. The 24-h accumulated precipitation height as obtained by (a) S30 (gray shaded) and S80 (dotted lines), and (b) S30C (gray shaded) and S30A (dotted lines). Maximum values are 4.3, 1.4, 1.1, and 4.5 mm for S30, S80, S30C, and S30A, respectively.

profiles of wind, humidity, and air and soil temperature as given in Mölders (2000). These profiles are attained by a dynamical initialization procedure. The large-scale pressure gradient is represented by a geostrophic wind of 7.5 m s^{-1} from 100° at a height of 10 km. Radiation is assumed to be for the 122d day of a year. The initial surface pressure, soil wetness factor, soil temperature at 1 m depth, and water surface temperature are set equal to 1003 hPa, 0.9, 285.0 K, and 282.6 K, respectively. This synoptic condition is oriented toward typical cases in spring, during which local recycling of previous precipitation can occur. The domain area is under the anticyclonic influence of a high over central Europe, with relatively warm weather conditions.

Simulations start at 0000 local time (LT) and are performed over 24 h. They are carried out by alternatively applying the land use data representative for either the 1930s or the 1980s. Additionally, nine simulations are performed with identical model configuration and initialization. They differ from S30 only insofar as one land use type (e.g., grassland) is altered to its full extent in S80 (Table 3). In these sensitivity studies, according to the definition by Mölders (2000), only simple land use changes occur (Table 3). Herein, simple land use changes are defined as the conversion of various land use types A, B, C, and so on, to only one land use type, D. Note that simulation S80 is the same as MIN and MIN750 in Mölders (1998, 2000) and Mölders (1999a), respectively.

b. Probability density functions

The statistical behavior of the response to the altered landscape is evaluated by frequency distributions of simulated water and energy fluxes, variables of state, and cloud and precipitating particles. Probability density functions are calculated by (Olberg and Rakóczi 1984; Mölders et al. 1996)

$$\mathrm{pdf}(\chi) = p(\chi \le X \le \chi + \Delta X)/\Delta X \qquad (1)$$

for the entire simulation time using the hourly data obtained by the different simulations at each grid point. Here, p is the frequency in the interval $(\chi, \chi + \Delta X)$. For each quantity regarded at reference height (e.g., wind, air temperature, humidity), which is located at a height of 10 m above ground, the probability density functions are based $50 \times 40 \times 24$ values. In the case of quantities regarded over the entire domain (e.g., cloud

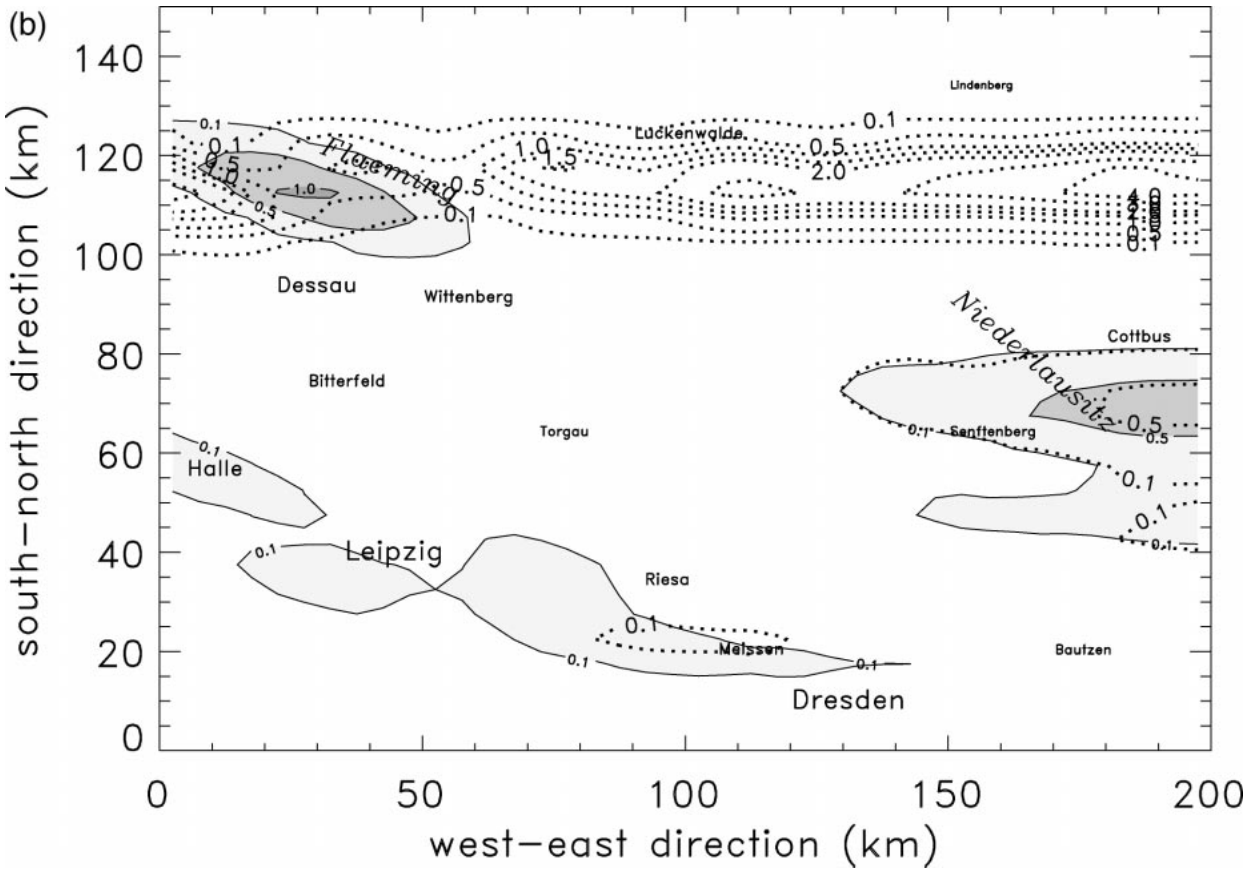

FIG. 3. (*Continued*)

water, rainwater, ice), the probability density functions are based on 50 × 40 × 16 × 24 values.

c. Similarity coefficients

Following Ogunjemiyo et al. (1997) and Friedrich (1999), Jackson et al.'s (1989) procedures for comparing data fields that contain differing parameters or for comparing data fields that have the same parameters but recorded at different times are adapted for comparing the results obtained by the simulations with the parameter sets that represent the landscapes of the 1930s and 1980s. The simulated quantities X_j at the grid point j on the distribution field are transformed into a set of values Z_j by subtracting the domain-averaged value and normalizing the difference by the standard deviation of the differences S:

$$Z_j = \frac{X_j - \overline{X}}{S}. \tag{2}$$

The similarity between two transformed distributions is now established on the basis of similarity in the sign of Z_j pairs as

$$C_s = \frac{m + n}{m + n + p}, \tag{3}$$

where C_s is the similarity coefficient; and n, p, and m are the numbers of Z_j pairs with negative, positive, and mixed signs. The similarity coefficient ranges from zero (no similarity) to one (absolute agreement). They indicate those land use changes to which the simulated quantities are the least sensitive. Furthermore, the time variance of similarity can be found. Note that the similarity coefficients determined for the distributions of thermal conductivity, heat capacity, emissivity, albedo, roughness length, field capacity, capillarity, and maximal evaporative conductivity of S30 and S80 amount to 0.78, 0.77, 0.79, 0.75, 0.76, 0.81, 0.84, and 0.83, respectively.

d. Detection of nonlinearity

The atmospheric response to concurrent land use changes may be more enhanced or less diminished when compared with those responses resulting from simple land use changes (e.g., Mölders 2000). In a linear response, at grid point j, the sum of the differentials

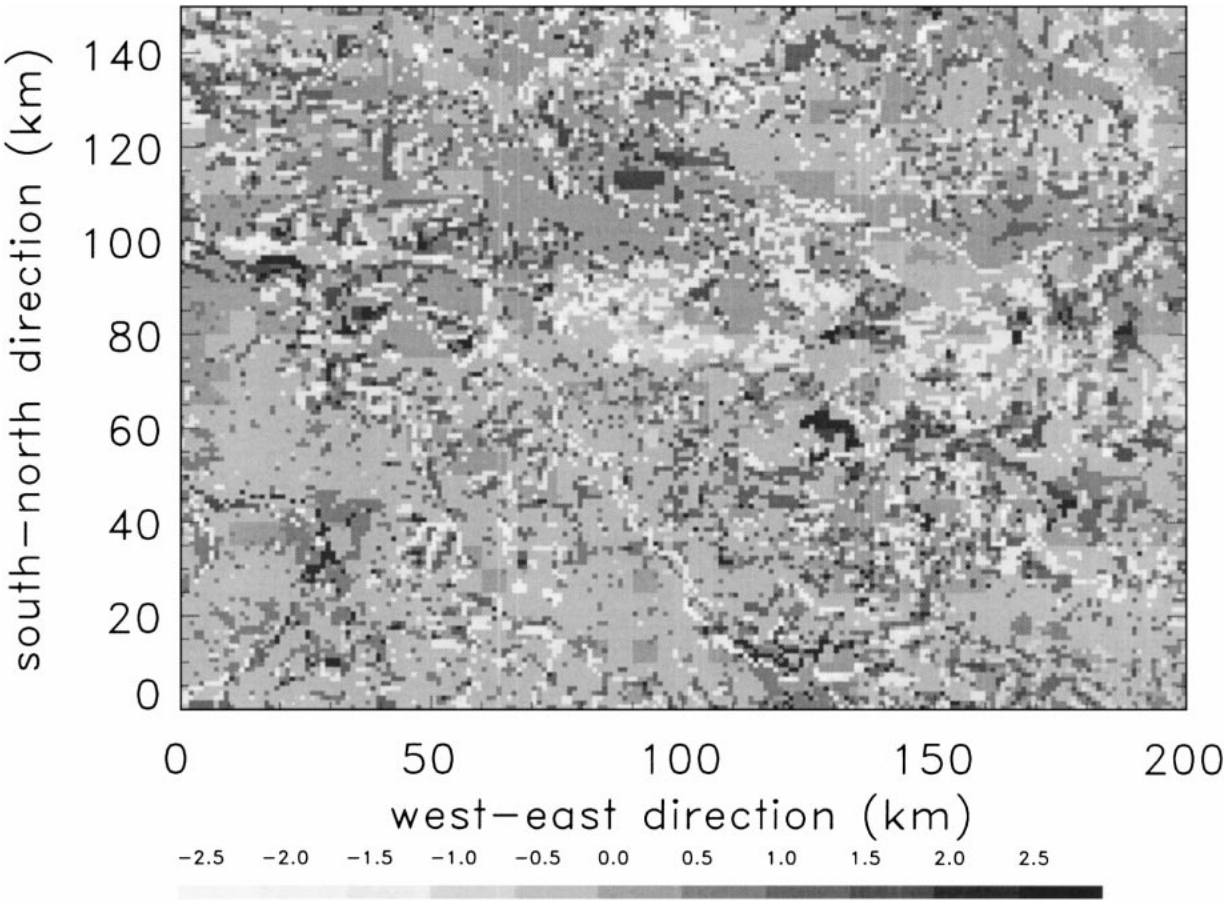

FIG. 4. Differences (S30 − S80) between the daily sums of evapotranspiration height (mm).

$\Sigma_{i=1}^{n}(X_j^k - X_j^i)$ in the simulated quantities X_j (e.g., water and energy fluxes), caused by simple land use changes, would equal the differentials $X_j^k - X_j^p$ in the atmospheric response to the concurrent land use changes (principle of superposition). Rearranging leads to (Mölders 2000)

$$(n-1)X_j^k - \sum_{i=1}^{n} X_j^i + X_j^p = \Delta \begin{cases} >0 & \text{enhancement} \\ =0 & \text{superposition} \\ <0 & \text{diminution.} \end{cases} \quad (4)$$

Here, the index k represents the simulation of the landscape at which point the changes start, namely, S30. Furthermore, $i = 1, \ldots, n$ stand for the simulations wherein only one land use type is altered to its extent in S80. Moreover, p represents the simulation with the concurrent land use changes, namely, S80. Enhancement means a positive deviation from the principle of superposition (Δ), and diminution is characterized by a negative one ($-\Delta$). To be discussed will be only those deviations from superposition whose absolute values amount to more than the margin for error that typically arises in routinely measuring the quantity X_j [i.e., $|\Delta| \geq 0.2$ K for air temperature, $|\Delta| \geq 0.5$ m s^{-1} for wind, $|\Delta| \geq 0.5$ g kg^{-1} for humidity (WMO 1971), $|\Delta| \geq 0.5$ K for ground temperature, and $|\Delta| \geq 35$ W m^{-2} for the fluxes (A. Raabe 1999, personal communication)].

4. Differences resulting from land use changes

The land use changes lead to a change in the degree of heterogeneity. By using the measure of heterogeneity defined by Mölders (1999a),

$$\delta_{\text{net}} = 0.5[\Phi/\Phi_{\max} + (X-1)/(X_{\max}-1)], \quad (5)$$

it can be found that the land use changes from the 1930s to the 1980s decreased heterogeneity from 0.53 to 0.41. This measure considers both the length of boundaries Φ between areas of different land use and the number of ecosystems X. For maximum heterogeneity ($\delta_{\text{net}} = 1$), each subgrid cell is also the boundary to another land use type, and, for homogeneity, there exists only one land use type and no boundary ($\delta_{\text{net}} = 0$). Here, $\Phi_{\max}$ is the total length of the possible boundaries, and $X_{\max}$ ($=16$) is the maximal number of various land use types that, in principle, may be distinguished by the land use datasets. Note that they do not all occur in the domains of interest of this study.

Important parameters in this study include roughness

length, maximum stomatal conductivity, and albedo Forests, villages, and settlements have greater roughness than the other land use types (Table 1). Because of the land use changes, the overall roughness length grows from about 0.39 to 0.43 m. Urbanization contributes to the most pronounced area-weighted change in roughness length (about 0.05 m). Maximum stomatal conductivity of forests is 42.5% lower than for grassland or agriculture. Thus, the land use changes lead to an overall increase of maximum stomatal conductivity of more than 14%. Coniferous forest, city, and marshland have the lowest albedo, and open-pit mines and grassland have the largest. Overall albedo increases slightly from 0.177 to 0.181. Open-pit mining and the villages increasing at the cost of agriculture play an important role in this increase.

The concurrent land use changes from the 1930s to the 1980s do not affect the simulated quantities of state, nor does the wind above the ABL, except in areas of deep convection. Similar results have been found for much smaller concurrent land use changes associated with future urbanization and various recultivation scenarios in this area (Mölders 2000). In S80, the domain-averaged daily temperature is 0.2 K higher, the domain-averaged daily humidity is 0.014 g kg^{-1} drier, the domain-averaged daily u and v components of wind are 0.06 and 0.1 m s^{-1} stronger, and the domain-averaged daily w (vertical) component is 0.2 cm s^{-1} weaker than in S30. Generally, the predicted fluxes vary more during the day, when the energetic input is high, than at night. In both landscapes, there is a higher water supply to the atmosphere over the forest-dominated northeastern part of the domain than over the agriculturally dominated southwestern part.

Because the landscape changes from the 1930s to the 1980s are greater than those assumed in Mölders's (2000) future scenarios, the effect on the microclimate, especially on evapotranspiration and precipitation, is greater than that reported in her study. Nevertheless, as will be shown later, the same areas are the most sensitive to the concurrent land use changes.

a. Surface temperatures, soil wetness, air temperatures, and humidity

The physical parameters of altered vegetation and soil (e.g., albedo, emissivity, capillarity, field capacity) affect surface temperatures both directly and indirectly. Changes in capillarity modify soil wetness, which again slightly affects soil temperature. Sensitivity studies show that an increase in albedo, for example, may slightly reduce cloudiness and precipitation as well as the extension of the areas receiving precipitation. Consequently, soil moisture increases and surface temperatures decrease where precipitation reaches the ground.

The probability density distribution of ground temperatures becomes steeper in response to the concurrent land use changes (Fig. 2). The appreciably different precipitation distribution and intensity of S80 (see also Fig. 3) lead to a shift in soil wetness factors toward lower values when compared with S30 (Fig. 2).

These altered surface temperatures and soil wetness factors modify the fluxes of sensible and latent heat (e.g., Figs. 4 and 5), vertical mixing, and cloudiness (e.g., Fig. 6). The modifications again affect the air temperatures of the ABL (Fig. 2). The probability density functions of the air temperatures at reference height show a trimodal distribution for S30 and S80 (Fig. 2). The often lower cloudiness in S80 (e.g., Fig. 6) contributes to air temperatures higher than in S30 (locally up to about 1–2 K). The trimodal structure (Fig. 2) corresponds mainly to the three land use types that prevail in the domain, namely, agriculture, grassland, and forest. The secondary maximum is shifted from about 9°C in S30 to about 9.5°C in S80 (Fig. 2), however. The minimum of probability that occurred for air temperatures about 8°C is more distinct in S80 than in S30. This change, among other things, is caused by the increased frequency of surface temperatures in the vicinity of 15°C. These higher surface temperatures mainly result from the decrease in grassland.

The probability of high specific humidity at reference height decreases because of the land use changes (Fig. 2). Only around noon, on average, is the near-surface atmosphere slightly drier in S30 than in S80, especially over Fläming and Niederlausitz. Note that, over large areas, at night the upper ABL of S30 is moister than in S80. Therefore, in S30, cloudiness increases compared with S80 (Fig. 6).

b. The wind vector

The vertically integrated negative buoyancy that a parcel must overcome by heating or mechanical means to convect freely is a function of the vertical velocity squared (e.g., Chase et al. 1999). Consequently, small changes in vertical motions can affect greatly the ability to initiate convection. A 5% increase in vertical velocity from 10 to 10.5 cm s^{-1}, for instance, enhances the negative buoyancy that a parcel can overcome by 10% and thus raises the potential for convection (e.g., Chase et al. 1999).

Usually, afforestation, open-pit mining, and urbanization increase surface roughness, and deforestation reduces it; that is, the concurrent land use changes alter the turbulent state of the atmosphere in both directions. When compared with S30, vertical mixing in S80 is reduced because of the lower proportion of forest and is intensified where urbanization occurs. Although the land use changes strongly modify the distribution of vertical motions, the probability density functions are barely altered (and are therefore not shown). The changes in land use slightly alter the horizontal wind field, leading to a lower probability of high v components and a higher probability of high u components, also not shown.

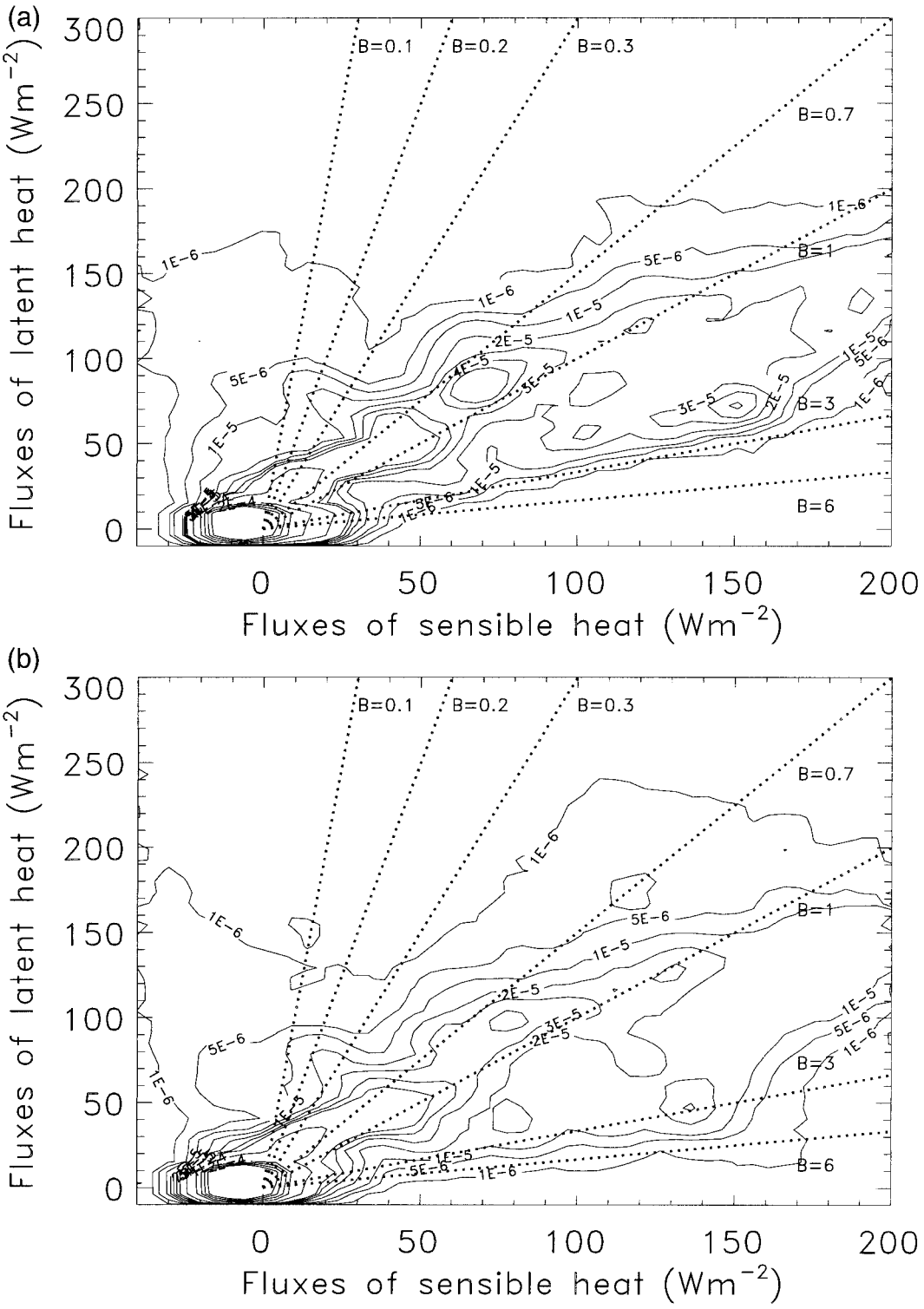

FIG. 5. Contour lines of joint probability density functions for the surface fluxes of latent and sensible heat in (a) S30, (b) S80, (c) S30C, and (d) S30A. Lines of constant Bowen ratios are superimposed.

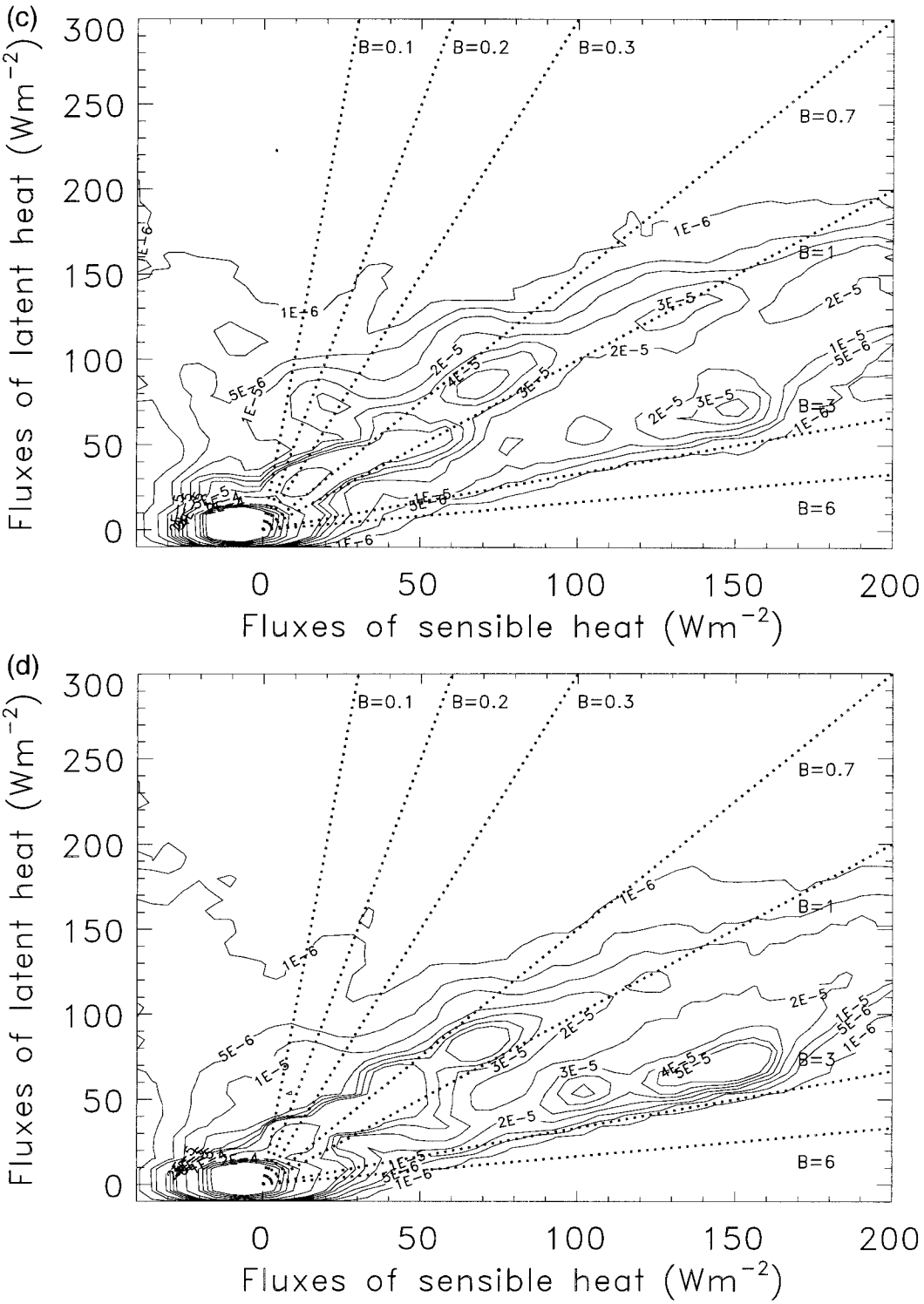

FIG. 5. (*Continued*)

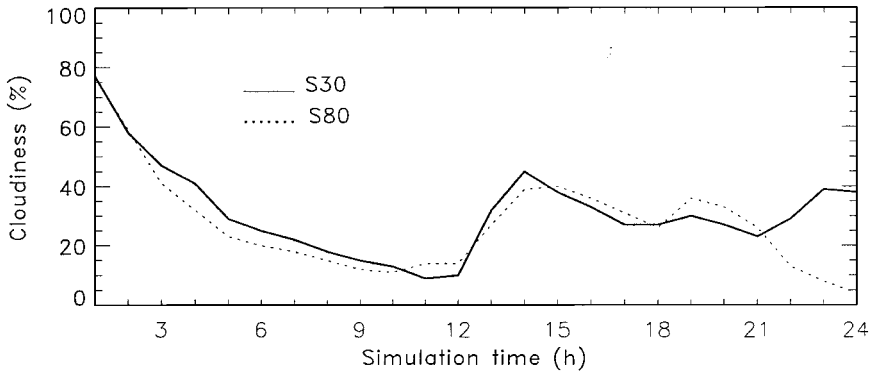

FIG. 6. Temporal development of cloudiness for S30 (solid lines) and S80 (dotted lines). Herein, cloudiness is given as percentage of the grid columns for which cloud water and/or ice exceed 0.001 g kg^{-1}.

c. The surface fluxes

As pointed out above, the modified physical parameters of plants and soil, among other things, affect the energy and water fluxes. A reduced albedo, for instance, leads to an increase in both the vertical motions and the fluxes of sensible and latent heat. On average, when compared with S30, in S80 less water vapor (domain average of 0.03 mm) is supplied to the atmosphere during the 24 h simulated. Maximum local decrease and increase amount to −2.6 and 2.5 mm, respectively. Usually, in S30, lower values occur over heath (usually a military site) or small open-pit mines than over the same areas in S80 (Fig. 4). Those areas in S30 that are covered by water or that are either sealed or altered to open-pit mines in the 1980s evapotranspire less in S80 (Fig. 4). Evapotranspiration rates also go down where grassland is converted to agriculture. On the contrary, the reverse land use change increases the water vapor supply to the atmosphere (Fig. 4). Evapotranspiration also differs where great discrepancies occur in the diurnal course of cloudiness as a result of the land use changes. The maximum 24-h accumulated evapotranspiration of S30 (2.93 mm) exceeds that of S80 (1.98 mm), and the minimum 24-h accumulated evapotranspiration of S30 (0.11 mm) is less than in S80 (0.2 mm).

The probability of moderate evapotranspiration rates decreases in S80, and that of high and low evapotranspiration rates slightly increases (Fig. 5). In comparison with S30, the probability density functions of sensible heat fluxes shift slightly toward lower values in S80, that is, the incoming energy is differently partitioned between sensible and latent heat in S30 and S80 (Figs. 5, 7).

Comparing the joint probability density functions of latent and sensible heat fluxes as obtained from the simulations using simple land use changes (Table 3) with those of S30 substantiates that land use changes in favor of coniferous forest (S80C) or grassland (S80G) provide a shift toward lower Bowen ratios (Fig. 5). On the other hand, when the land use changes from forest or grassland in favor of open-pit mining, agriculture, village, or city, the reverse is true and therefore leads to greater Bowen ratios (Fig. 5). Note that the other simple land use changes hardly affect the joint probability functions.

In S80, the probability density functions of soil heat fluxes shift toward values lower than in S30 (Fig. 7).

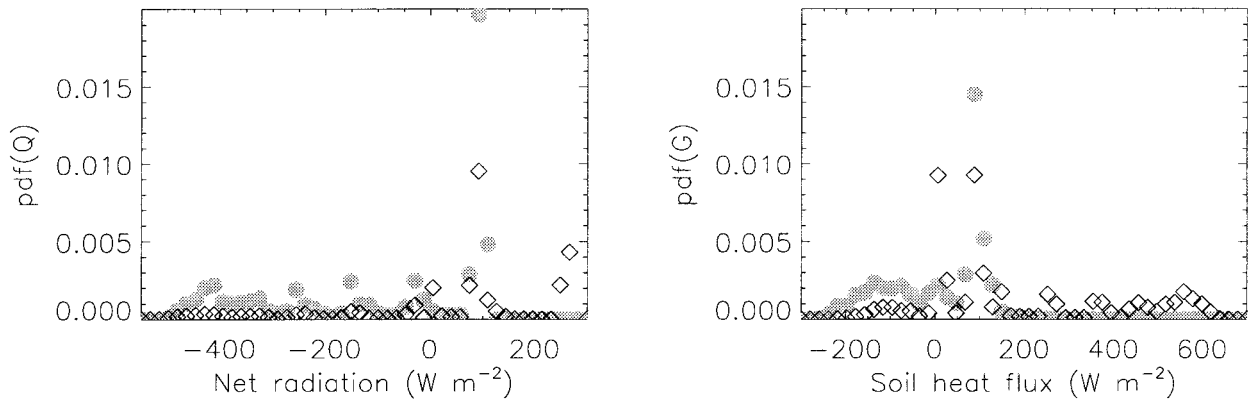

FIG. 7. Comparison of probability density functions of (left) net radiation Q and (right) soil heat fluxes G as determined by S30 (gray circles) and S80 (diamonds).

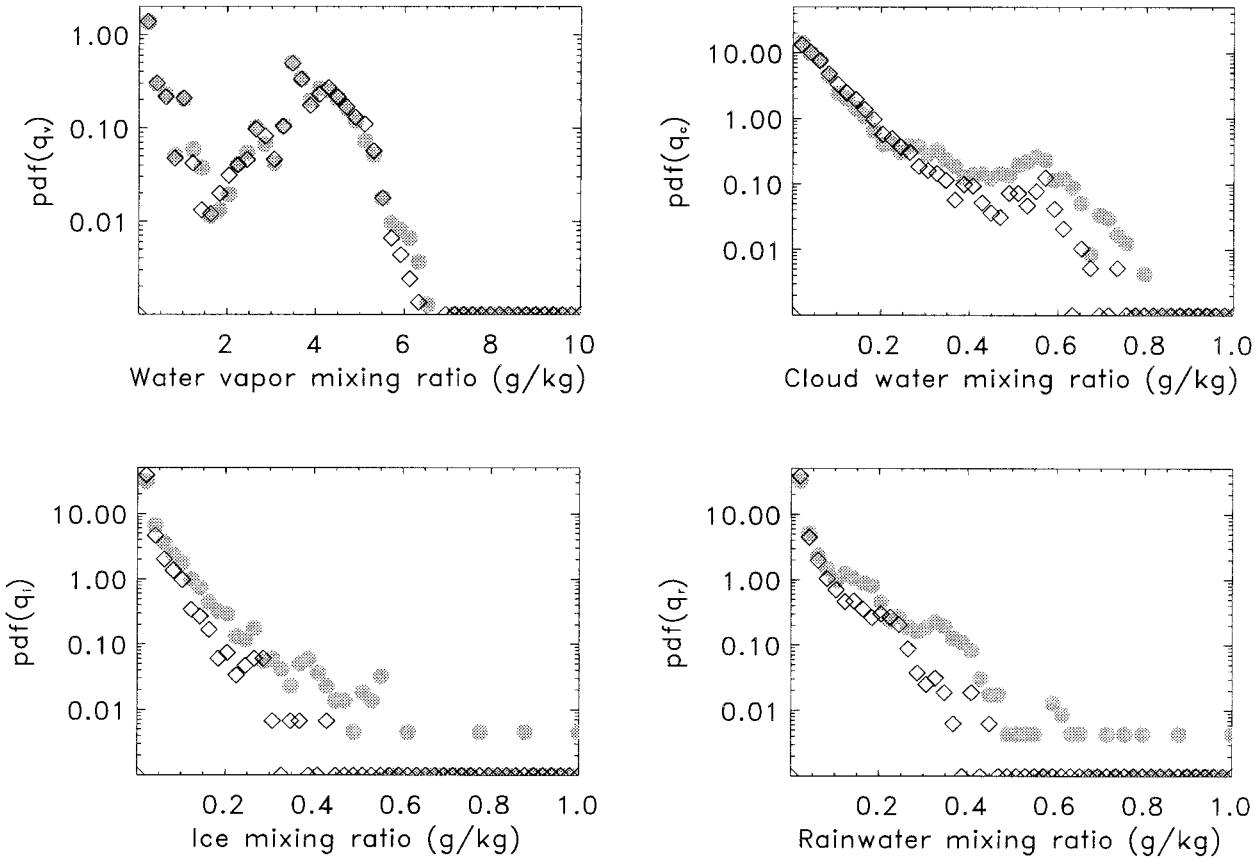

FIG. 8. Comparison of probability density functions of water vapor q_v, cloud water q_c, ice q_i, and rainwater q_r within a column (upper left to lower right) as determined for S30 (gray circles) and S80 (diamonds). Note that y axis is logarithmic.

Although in S80 the probability density distribution of net radiation is smoothed out, that of the soil heat fluxes gets more textured (Fig. 7). This effect results partly from the altered cloudiness (Fig. 6). The probability density functions of soil heat fluxes and net radiation are altered more strongly by the land use changes than those of latent and sensible heat fluxes (Figs. 5 and 7). Looking at the distributions of net radiation shows that net radiation reacts very sensitively to the modified cloudiness.

d. Cloud and precipitating particles

In the morning, early afternoon, and at night, the cloudiness in S30 exceeds that of S80, whereas in the late afternoon, it is usually less than in S80 (Fig. 6). The enhanced evapotranspiration in S30 occurring in the afternoon contributes to the increased precipitation in the late evening hours, to the altered precipitation distribution (Fig. 3), and to the increased cloudiness at night as compared with S80 (see Fig. 6). The aforementioned altered vertical mixing also contributes to the change in cloud and precipitation formation. In the morning, the greater cloudiness in S30 (Fig. 6) results from the more unstable stratification locally as compared with S80. The large differences in cloudiness at night reflect that in S80 clouds exist only over the water meadows of Elbe at Riesa and over Oberlausitz, but in S30 two largely east–west-oriented cloud banks exist in the northern and southern part of the domain (not shown). These cloud banks still contain slight amounts of rainwater at some locations, but in S80 no rainwater exists.

As shown for synthetic landscapes, the amount of cloud water may be modulated strongly by the degree of heterogeneity and the arrangement and size of the patches of the underlying surface (Friedrich and Mölders 2000). Sensitivity studies showed that increasing roughness length may cause a change in the position of the cloud and precipitation fields. For the land use changes examined here, the altered degree of heterogeneity and the related modified aerodynamic roughness also contribute to the great differences in the distributions of clouds (e.g., Fig. 6) and precipitation (Fig. 3). There are fewer cloud and precipitation particles in S80 than in S30 (Fig. 8). As compared with S30, the probability density functions in S80 of water vapor, cloud particles, and precipitating particles shift toward lower values (Fig. 8). Nevertheless, S80 provides a more showerlike precipitation with higher intensities locally

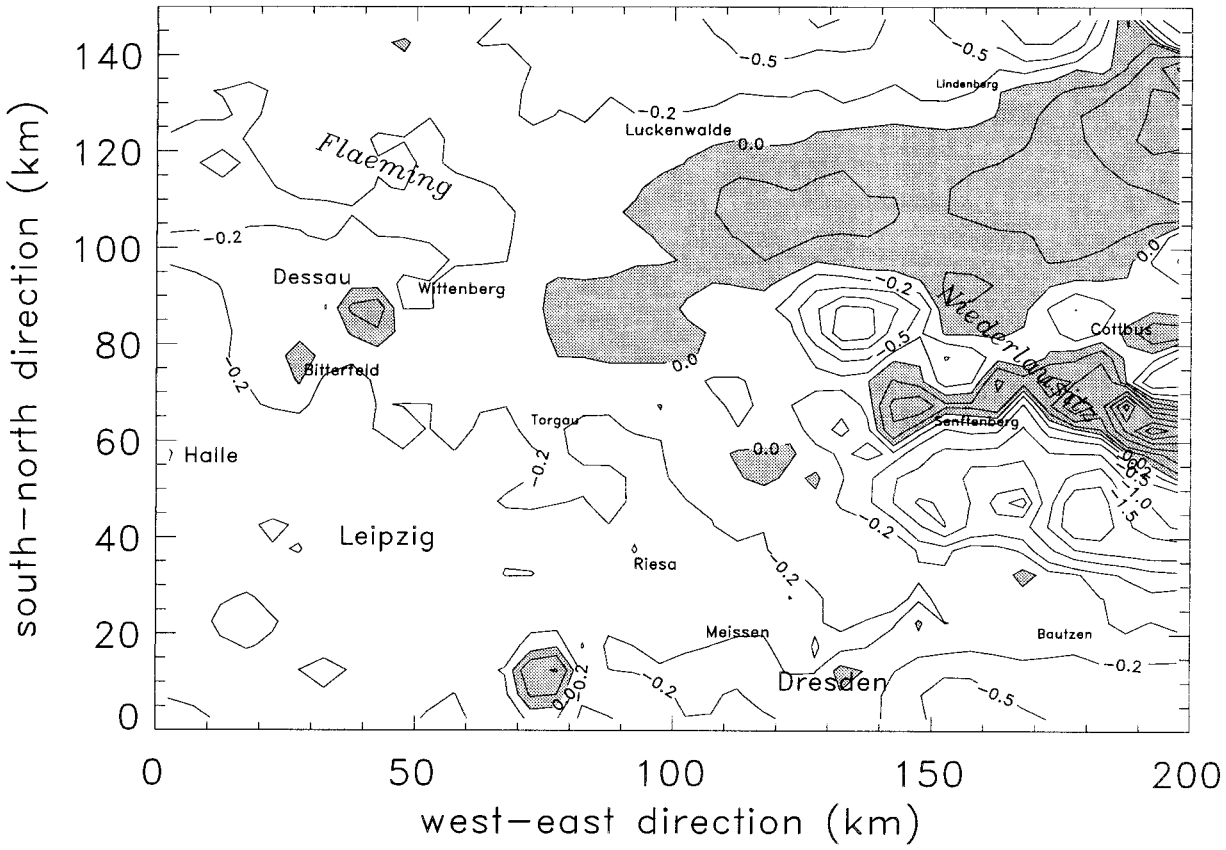

FIG. 9. Differences Δ (K), according to Eq. (4) for air temperatures at reference height at 1200 LT. The gray and white patches represent positive and negative deviations from superposition, respectively. Areas of relevant deviations from superposition are indicated by the contour lines.

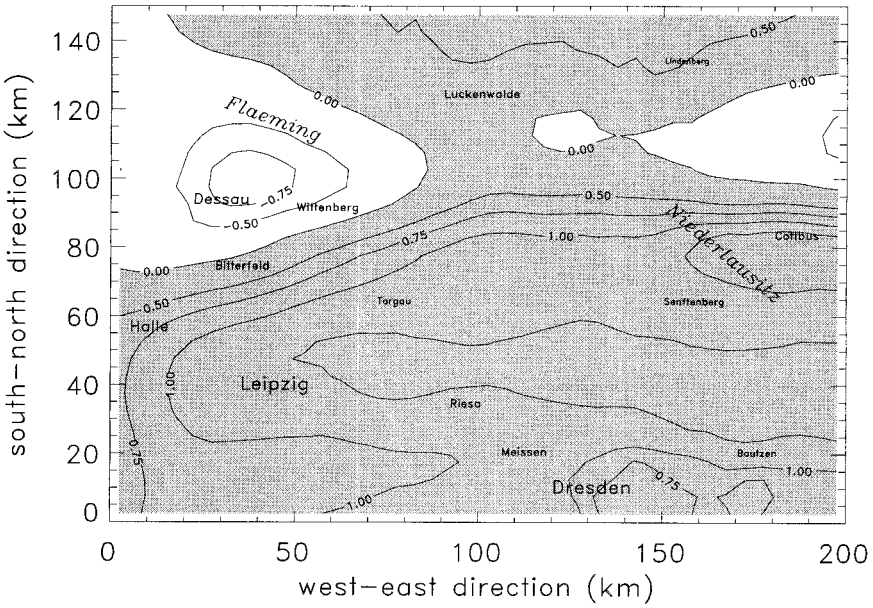

FIG. 10. As in Fig. 9 but for differences Δ (g kg^{-1}) in humidity at reference height at 2400 LT.

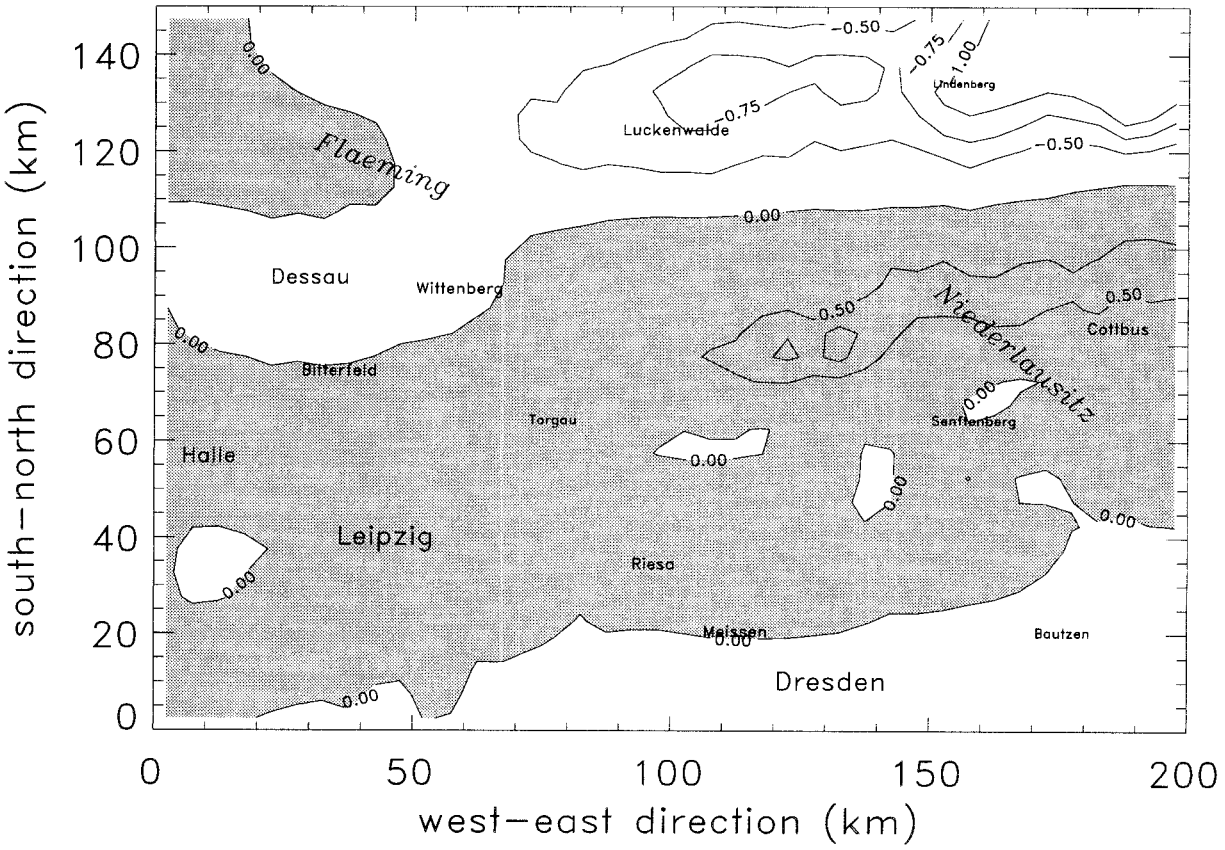

FIG. 11. As in Fig. 9 but for differences Δ (m s^{-1}) in the v component of the wind vector at reference height at 1200 LT.

than does S30. The domain-averaged accumulated precipitation of S30 exceeds that of S80. Consequently, the probability density functions of precipitation and soil wetness shift toward lower values (see also Fig. 2).

The altered heating, vertical mixing, and moisture supply lead to a modified partitioning between the microphysical paths of precipitation formation. Because of the latter modifications, the consumption of heat and the release of latent heat, and thus air temperatures, are affected. Consequently, the vertical motions are modified further by the interaction of microphysics and dynamics.

The saturation pressure above ice is lower than that above water. This difference is at a maximum at about −15°C. Thus, at cloud tops, the difference between the saturation pressure above ice and water is greater in S30 than in S80 because of the cooler ABL of the former than the latter. If saturation pressure in a cloud is below that of water but above that of ice, ice will grow at the expense of cloud water [note that a mass-weighted specific saturation mixing ratio is used in the bulk parameterization of cloud microphysics (see Mölders et al. 1997a)]. For the reasons given above, more water vapor is converted to ice in the moister and cooler ABL of S30 than in that of S80 (e.g., Figs. 2 and 8). Because only a few cloud condensation nuclei act as ice nuclei (e.g., Heymsfield and Sabin 1989), and, hence, the size distributions of ice clouds are spread over few large particles, quickly developing fall speeds of tens of centimeters per second (e.g., Heymsfield 1977), sedimentation is immediately considered after ice has been formed (e.g., Mölders et al. 1997a). Consequently, the greater amount of ice in S30 leads to an increase in sedimentation of ice. As a result, ice quickly reaches those areas of the ABL where temperatures are warmer than the freezing point and then melts. Thus more rainwater is built up by the cold path of precipitation formation in S30 than in S80. Consequently, at some locations, precipitation starts about 2 h earlier in S30 than in S80, which also contributes to the different precipitation distribution (Fig. 3). In the warmer clouds of S80, coalescence and riming are favored. Thus, when compared with S30, a more showerlike precipitation may establish itself in areas of strong moisture convergence. The precipitation distributions obtained by the sensitivity studies assuming simple land use changes show that, of all other simple land use changes, changing the distribution of coniferous forest (high roughness) or agriculture (low roughness) affects the distribution of precipitation to the greatest degree (e.g., Fig. 3). This finding may suggest that, in this case study, the altered vertical mixing appreciably contributes to the change in

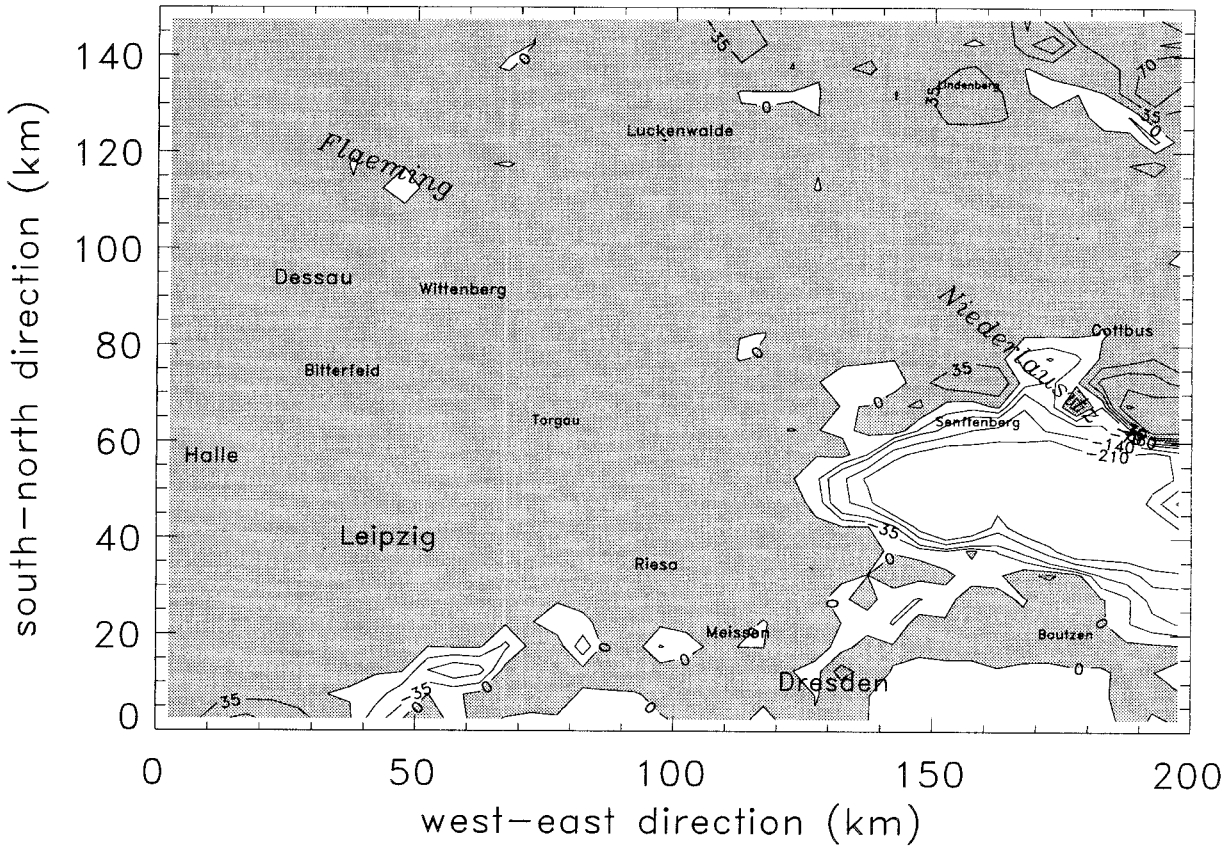

FIG. 12. As in Fig. 9 but for differences Δ (W m^{-2})in latent heat fluxes at 1200 LT.

the position of precipitation distribution. Note that the shift in the position of the precipitation fields is of similar magnitude to that found by Chase et al. (1999) for the Colorado Rocky Mountains in response to the land use changes in the Great Plains.

5. Discussion of enhancements and diminution

a. Surface temperatures, soil wetness, air temperatures, and humidity

Large negative deviations from superposition occur for surface temperatures in areas where cloudiness is altered strongly by land use changes (not shown). At noon in southern Niederlausitz, for instance, surface temperatures are more than 3 K lower than expected for a linear behavior, whereas at night, the great negative deviation in surface temperature and cloudiness seems to be related to those areas of land use changes that have a great increase in surface roughness (e.g., by urbanization or afforestation). During the day, appreciable positive deviations occur where large areas of agriculturally used land are changed to grassland, whereas they are found over Fläming at night.

Although there is a linear behavior for soil wetness before the onset of precipitation, afterward it is nonlinear. After 24 h of simulation, soil wetness of S80 is enhanced in comparison with the superposition in the differences of simple land use changes (not shown). The areas of enhancement correspond to those of high precipitation amounts in S30 and S30A (e.g., Fig. 3).

In Niederlausitz, a strong nonlinear behavior of air temperatures at reference height is found at noon (Fig. 9). Here, diminution and enhancement alternate on a distance of less than 100 km. One time only does diminution occur over areas dominated by agriculture and grassland in the 1930s and by agriculture only in the 1980s (cf. Figs. 1 and 9). In the other case, diminution occurs in S30 over areas mainly covered once by forest that partly changed to lakes, agriculture, and settlements (cf. Figs. 1 and 9). On the contrary, at reference height, air temperatures are enhanced in an area where forests still existing in the 1930s are already eliminated in the 1980s. Enhancement occurs in an area (center at 120 km, 110 km) where only slight afforestation is found (cf. Figs. 1 and 9). At night in Fläming, air temperatures at reference height deviate positively (up to 1.1 K) from superposition. Negative deviations (locally up to −5.9 K) occur in nearly all the rest of the domain. Note that, in an environment dominated by agriculture, urbanization tends to cause slightly higher temperatures than expected from superposition (cf. Figs. 1 and 9).

Whereas, in Mölders's (2000) studies on future land

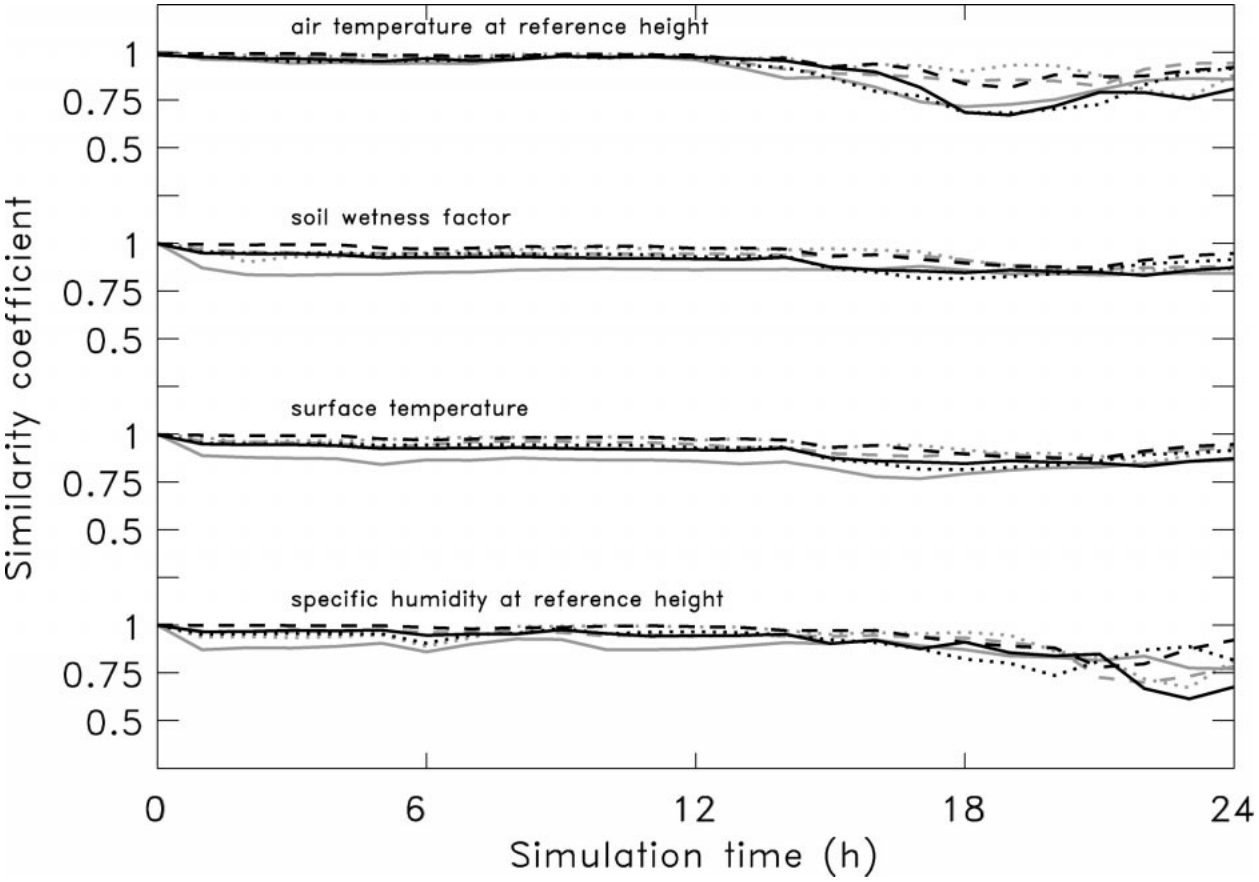

FIG. 13. Temporal development of similarity coefficients as obtained for specific humidity and air temperature at reference height, surface temperatures, and soil wetness factors for the concurrent land use changes from S30 to S80 (gray solid lines), for S30 to S30W (gray dotted lines), S30 to S30G (gray dashed lines), S30 to S30A (black solid lines), S30 to S30D (black dashed lines), and S30 to S30C (black dotted lines), respectively.

use changes, humidity at reference height shows a linear behavior, for the much larger concurrent land use changes from the 1930s to the 1980s it does not. In the recent study, at noon, for instance, humidity at reference height diminishes (more than -0.5 g kg^{-1}) in the region around Lindenberg (not shown). Here, deforestation, especially in favor of agriculture and settlements, has taken place. Moreover, secondary differences result from modified cloudiness. In the agriculturally dominated part of the domain, however, humidity at reference height hardly deviates from superposition. At night in Fläming, humidity at reference height is up to 0.9 g kg^{-1} lower than expected from superposition (Fig. 10). In Niederlausitz, on the other hand, in the surroundings of Leipzig and Lindenberg, humidity at reference height exceeds the values expected for a linear behavior (up to 1.6 g kg^{-1} at maximum; Fig. 10). The modified evapotranspiration, evaporation of raindrops, and the resultant cooling mainly contribute to these differences because of the nonlinear relationship of specific saturation and air temperature.

b. The wind vector

For the small concurrent land use changes assumed for the future, no relevant nonlinearity has been found for the u and v components of the wind vector (Mölders 2000). When compared with superposition for the land use changes that took place from the 1930s to the 1980s, the u component of the wind vector is enhanced in afforested areas of Fläming, and its v component is enhanced in afforested areas of Niederlausitz (e.g., Fig. 11). Comparing these findings with that of Mölders (2000) suggests that concurrent land use changes have to take place over large areas to provide a nonlinear response in the horizontal wind field.

The w component of the wind vector does not deviate from superposition. Note that, since the vertical velocities are volume averages that represent volumes of the model layer thickness times 5 km $\times$ 5 km, the magnitude of vertical velocity depends on grid size. Generally, the inclusion of a finer grid increases the ability of meteorological models to produce larger vertical motions and thus differences caused by land use changes,

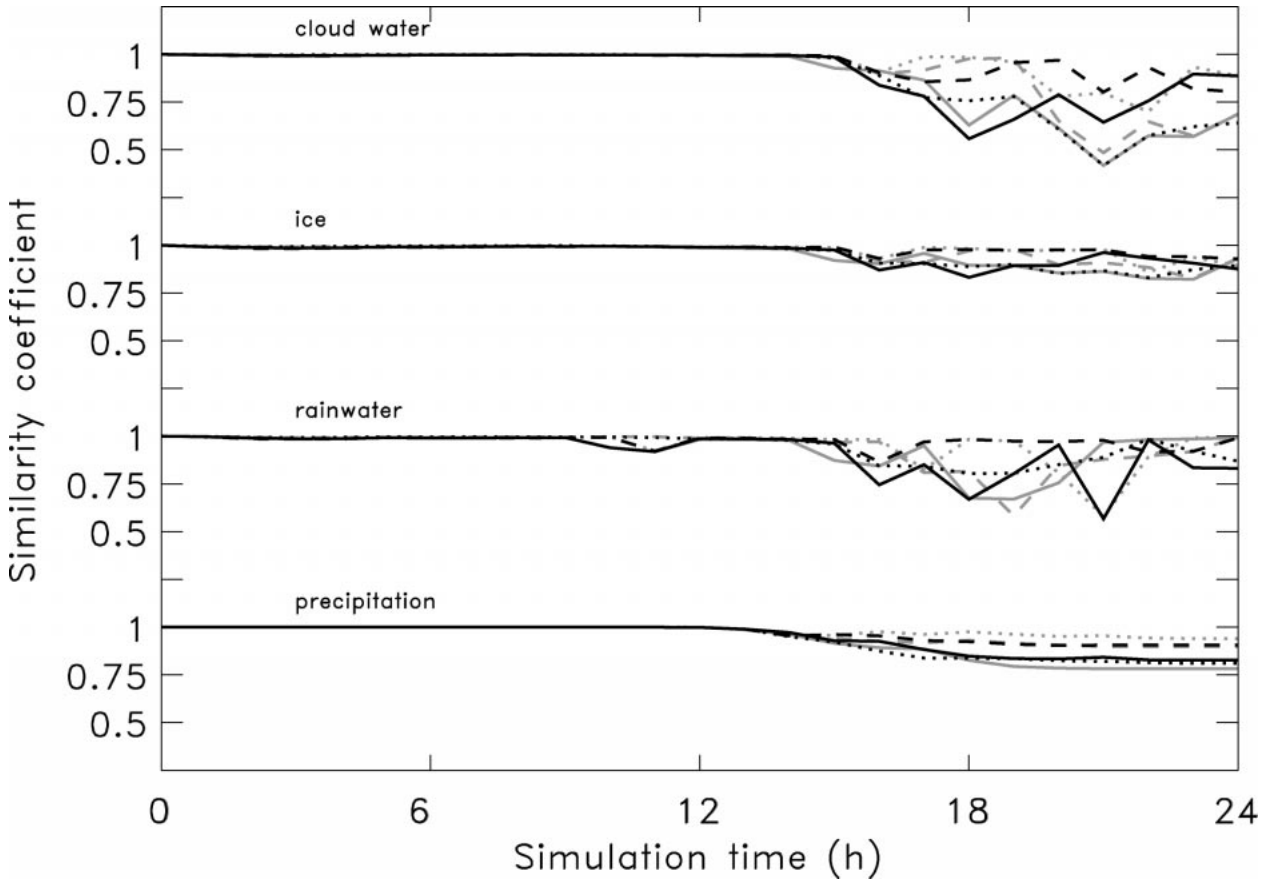

FIG. 14. As in Fig. 13 but for the cloud and precipitating particles as well as precipitation.

because small-scale horizontal temperature gradients and velocities can be resolved (Friedrich and Mölders 2000).

c. The surface fluxes

At noon in southern Niederlausitz, the fluxes of latent and sensible heat are diminished (by more than 210 W m^{-2}), as are the air temperatures and humidity at reference height (e.g., Fig. 12). At night in the Sächsische Bergland (area southeast of Leipzig to Dresden), however, sensible heat fluxes deviate positively (up to 39 W m^{-2}) from superposition. In this case, latent heat fluxes deviate negatively (up to -69 W m^{-2}) in the conurbation of Dresden.

At noon in southern Niederlausitz, soil heat fluxes of S80 are up to 195 W m^{-2} higher than expected from superposition. In the Lindenberg area, positive deviations from superposition also exist (not shown). At night, however, soil heat fluxes are enhanced (more than 35 W m^{-2}) in the Sächsische Bergland, whereas they are diminished in Fläming (not shown). These changes, among other things, may be attributed to altered optical cloud thickness and altered cloud coverage (Fig. 6).

Despite the great changes in cloudiness (e.g., Fig. 6), no relevant deviations from superposition exist for net radiation.

d. Cloud and precipitating particles

In Niederlausitz, positive and negative deviations from superposition occur for ice that may be explained by secondary effects. The altered surface conditions in S80, on average, lead to reduced moisture and enhanced heat supply to the atmosphere. As a result, cloudiness decreases (e.g., Fig. 6). Moreover, less cloud and precipitating particles are built up. At the same time, the partitioning between the warm and cold paths of cloud microphysics shifts toward a higher preference for the warm phase path. The modified cloud particles affect insolation and again the surface fluxes. If cloudiness decreases in S80 as compared with S30, evapotranspiration may increase. Nevertheless, as discussed above, often less water evapotranspires in S80 than in S30. Because of feedback processes between evapotranspiration and cloudiness, the temporal development of the cloud and precipitation particles differs appreciably. As pointed out above, the high nonlinearity results from the nonlinear relation of temperature and saturation

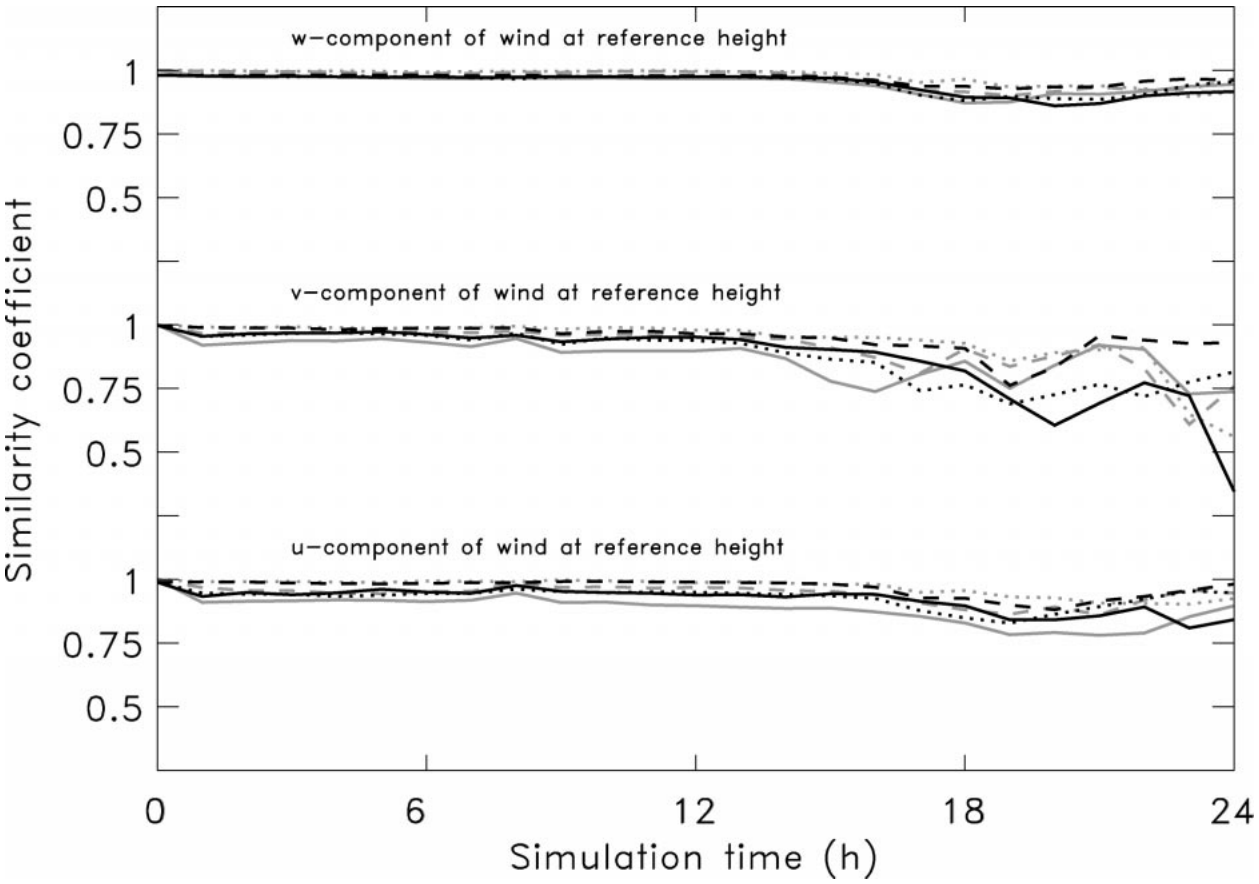

FIG. 15. As in Fig. 13 but for the components of wind vector.

pressure and from the different (temperature dependent) saturations above ice and water, respectively.

6. Discussion of similarity

a. Surface temperatures, soil wetness, air temperatures, and humidity

The distributions of surface temperature are the most dissimilar for concurrent land use changes, followed by simple land use changes in favor of agriculture or coniferous forest (Fig. 13). As discussed above, the altered distributions of cloudiness, precipitation, and soil wetness play roles that are, on average, more affected by these land use changes than by others (e.g., Fig. 14).

Before the onset of precipitation, the greatest dissimilarities in the distributions of soil wetness factors occur for the concurrent land use changes (Fig. 13). It is after the onset of precipitation, however, that the simple land use changes in favor of agriculture or coniferous forest cause dissimilarities greater than those from all other land use changes.

On average, the greatest dissimilarity in the air temperatures at reference height in S30 occurs for the simulation in which only agricultural land or coniferous forest change to their S80 extent, followed by concurrent land use changes (Fig. 13). At reference height, the distribution of humidity in S30 is the most dissimilar to that provided by S80 or the simulations in which only water, grassland, agriculture, or deciduous forest are converted to their S80 extent (Fig. 13). The greatest disparity between the specific humidity or air temperatures at reference height in any 24-h period occurs in the late afternoon and after sunset (Fig. 13). These greater dissimilarities result from secondary effects, namely, the evaporation of rainwater and the related evaporative cooling.

b. The wind vector

The modeled wind fields show a higher similarity before and around noon than after that time (Fig. 15). In S30, both the cooling resulting from evaporation of rainwater and the settling of rainwater contribute to downward motions (interaction of microphysics and dynamics) after the onset of precipitation. Consequently, the similarity in the fields of vertical motions then decreases (cf. Figs. 6 and 15). At that time, secondary differences in the horizontal wind field result from outflow of air in the downdrafts of precipitating clouds and thereby reduce similarity between S30 and S80.

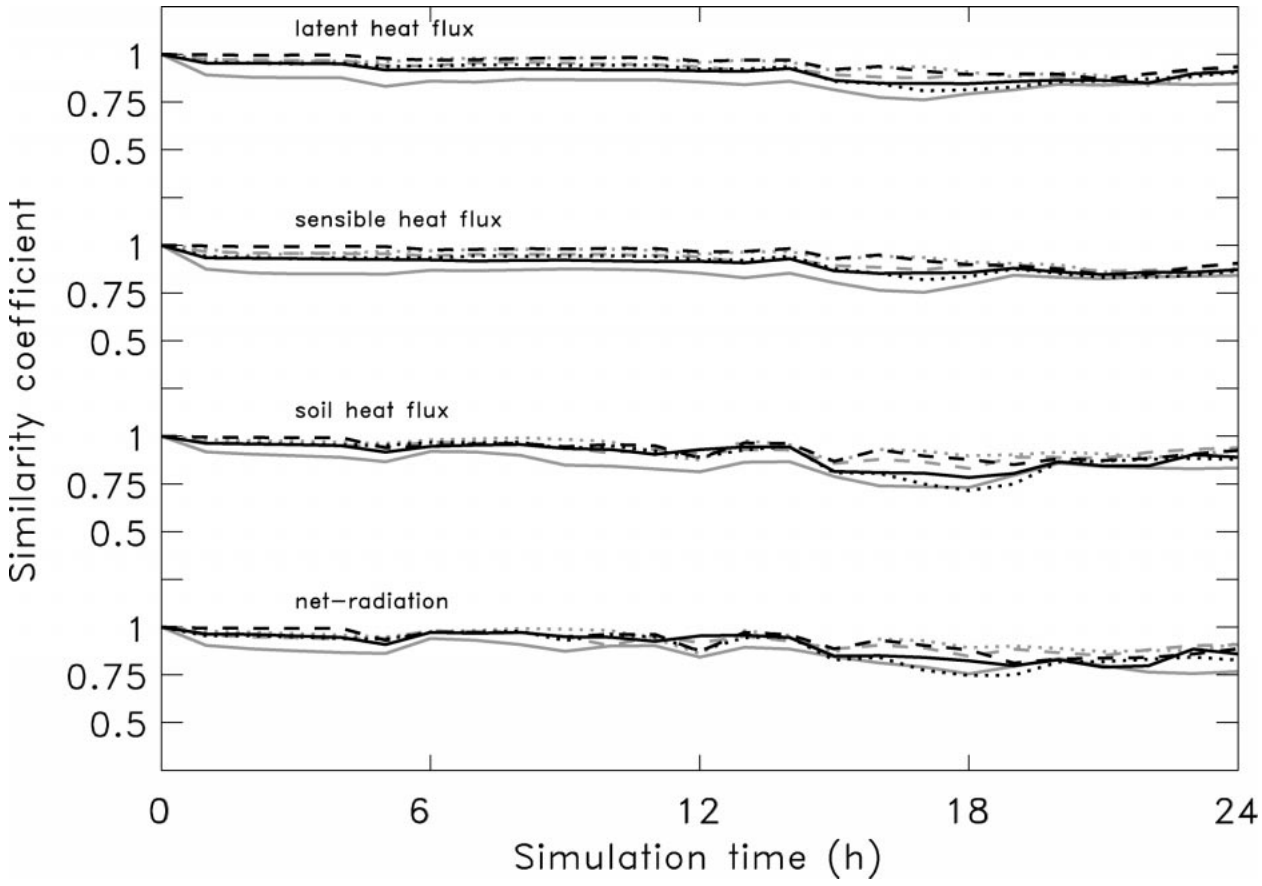

FIG. 16. As in Fig. 13 but for the surface fluxes.

Up until the late afternoon, S80 shows the least similarity to S30 for the horizontal components of the wind vector (Fig. 15). Later on, however, S30C and S30A provide fewer similarities to S30 for the v and w components of the wind vector than for those of S80. Land use changes that favor coniferous forest contribute especially to a high degree of change in vertical motions. Their effect, however, is mitigated by the other concurrent land use changes in S80.

c. The surface fluxes

On average, the modeled distributions of sensible and latent heat fluxes are more similar than those of net radiation or soil heat fluxes (Fig. 16). In the latter case, the greatest dissimilarities exist between S30 and S80 (Fig. 16). Note that net radiation and soil heat fluxes react more sensitively than the latent and sensible heat fluxes to altered cloudiness, in comparison with their relative reactions to land use changes (Fig. 16). The similarity coefficients obtained by comparing the S30 results with those of simulations having simple land use changes show that it is land use changes in favor of agriculture and coniferous forest that mainly contribute to the dissimilarities (Fig. 16). On average, the obtained fluxes agree more closely with those yielded by S30 in the early morning than in the late afternoon and early evening (Fig. 16).

d. Cloud and precipitating particles

In comparing S30 and S80, the column-averaged similarity coefficients of cloud and precipitating particles indicate that the modeled ice mixing ratios are more similar than those of cloud water and rainwater (Fig. 14). The similarity coefficients indicate the strong effect on cloud water that concurrent land use changes and simple land use changes in favor of coniferous forest, grassland, or agriculture have (Fig. 14). The dissimilarities grow, with increasing integration time, after the onset of precipitation (cf. Fig. 14). Then the precipitation fields predicted by S30M, S30O, S30W, S30G, S30D, S30V, and S30T broadly agree with those of S30 (see also Fig. 14). By contrast, there is little agreement between the precipitation obtained by S30 and that yielded by S30C, S30A, and S80 (Fig. 14).

7. Conclusions

Numerical simulations alternatively assuming landscapes of the 1930s and the 1980s are made at timescales

relevant for micrometeorological processes to examine the influence of land use changes on these microclimatically relevant processes. Sensitivity studies are performed in the landscape of the 1930s wherein one land use type is altered according to its distribution in the 1980s.

The results obtained for the landscape of the 1980s show a spatial and temporal change in water availability and vertical motions as compared with those yielded with the landscape of the 1930s. Consequently, the simulated distributions and accumulated amounts of precipitation differ appreciably for the two landscapes. These differences are of special interest for the microclimatic conditions and local recycling of previous precipitation. A slight increase in vertical motion may be decisive for convection to occur. A precipitation event in the early afternoon, for instance, contributes more to evapotranspiration and thus local recycling than to runoff, and at night the opposite is true. Thus, the earlier onset of precipitation at some locations in S30, among other things, not only contributes to a different precipitation distribution but also leads to an increase in 24-h accumulated precipitation.

Application of the principle of superposition shows that Niederlausitz and Fläming (both dominated by high vegetation and some grassland) are more sensitive to land use changes than are the other parts of the domain. A similar behavior was found by Mölders (2000) for land use changes expected in the future. A look into the areas of greatest deviation from superposition suggests that the patch size of homogeneous land use made after the land use changes is decisive to getting a nonlinear response.

Deviations from superposition of surface temperature, sensible heat flux, soil heat flux, and net radiation occur in areas where large differences in cloudiness occur. This finding means that concurrent land use changes may alter nonlinearly the temporal course of the energy and water cycles. Moreover, deviation from superposition may also result from secondary effects.

The same kind of land use changes may provoke another atmospheric response in different surroundings (see Niederlausitz). Thus, one has to conclude that the prevailing land use next to the converted areas influences the effects of land use changes. Consequently, the land use that prevails in the environment of foreseen land use changes also has to be considered in authorization procedures.

The differences found in air temperatures at reference height, surface temperatures, precipitation, and cloudiness suggest that, in areas of big land use conversions, changes in these quantities could be detectable if stations were installed at these sites. Thus, here and in regions of great nonlinear response, climate stations should be installed to evince the effect of land use changes on climate by observational data. Unfortunately, historical data are rare. Nevertheless, the decadal means of observed air temperature at Dresden and Görlitz (Oberlausitz) show the same ratio between the values of the 1930s and the 1980s as was found for the grid cells of these locations in the simulations. The observed decadal mean precipitation, however, decreases for Görlitz and increases for Dresden (see *Meteorologischer Dienst* for 1950 and 1980–89).

The results of the simulations with the simple land use changes manifest that the magnitude of atmospheric response to land use changes does not necessarily depend on the fraction of the domain that experiences land use conversions. In addition to the size of patches where the individual changes take place, the contrast in the hydrologic and thermal behavior of the changes is decisive for the magnitude of response. Considering the similarity coefficients, it may be concluded that the altered albedo and roughness length play roles especially.

To improve understanding of the effect of concurrent land use changes on local climate, future studies should examine whether concurrent land use changes provide a different response to the atmosphere under different climate conditions. Moreover, it has to be examined to what degree land use changes contribute to recent climate changes. Therefore, one should investigate whether the nonlinearity and significance of the effects also exist in the long term (e.g., week, month, vegetation period, hydrological year, or climate scale) as was found for the large (e.g., Copeland et al. 1996) and regional scales (e.g., Pielke et al. 1999). If such clues are detected, regional climate simulations will urgently require sophisticated biome models that are run on subgrid scales to evaluate correctly the climatic effects on water resources. Additionally, uncertainty analysis on the influence of anthropogenic land use changes and examination of the relative contribution of these land use changes to climate change are urgently needed.

Acknowledgments. I express my thanks to K. Fröhlich and K. Friedrich for digitizing the land use data. The historical vegetation and soil limits were derived from digitized historical topographic maps of Saxony, Saxony–Anhalt, Thuringia, and Brandenbourg. I thank G. Kramm, K. E. Erdmann, A. Raabe, A. Ziemann, D. P. Lettenmaier, and the anonymous reviewers for fruitful discussions and helpful comments. Furthermore, I thank N. Röhrs for help with the language. Thanks also to the DFG for financial support of this study under Contracts Mo770/1-1 and Mo770/1-2.

REFERENCES

Anthes, R. A., 1984: Enhancement of convective precipitation by mesoscale variations in vegetative covering in semiarid regions. *J. Climate Appl. Meteor.,* **23,** 541–554.

Calder, I. R., R. A. Hall, H. G. Bastable, H. M. Gunston, O. Shela, A. Chirwa, and R. Kafundu, 1995: The impact of land use changes on water resources in sub-Saharan Africa: A modelling study of Lake Malawi. *J. Hydrol.,* **170,** 123–136.

Chase, T. N., R. A. Pielke Sr., T. G. F. Kittel, J. S. Baron, and T. J. Strohlgren, 1999: Potential impacts on Colorado Rocky Moun-

tain weather due to land use changes on the adjacent Great Plains. *J. Geophys. Res.,* **104,** 16 673–16 690.

Claussen, M., 1988: On the surface energy budget of coastal zones with tidal flats. *Contrib. Atmos. Phys.,* **61,** 39–49.

——, 1997: Modeling bio-geophysical feedback in the African and Indian monsoon region. *Climate Dyn.,* **13,** 247–257.

Copeland, J. H., R. A. Pielke, and T. G. F. Kittel, 1996: Potential climatic impacts of vegetation change: A regional modeling study. *J. Geophys. Res.,* **101,** 7409–7418.

Cotton, W. R., and R. A. Pielke, 1995: *Human Impacts on Weather and Climate.* Cambridge University Press, 288 pp.

Devantier, R., and A. Raabe, 1996: Application of a quasispectral cloud parameterization scheme to a mesoscale snowfall event over the Baltic Sea. *Contrib. Atmos. Phys.,* **69,** 375–384.

Eagleson, P. S., 1982: Ecological optimality in water-limited soil-vegetation systems: 1. Theory and hypothesis. *Water Resour. Res.,* **18,** 323–340.

Eppel, D. P., H. Kapitza, M. Claussen, D. Jacob, W. Koch, L. Levkov, H.-T. Mengelkamp, and N. Werrmann, 1995: The non-hydrostatic mesoscale model GESIMA. Part II: Parameterizations and applications. *Contrib. Atmos. Phys.,* **68,** 15–41.

Friedrich, K., 1999: Numerische Untersuchungen zur Sensitivität des Bowen-Verhältnisses (Numerical investigations on the sensitivity of the Bowen ratio). M.S. thesis, Institut für Meteorologie, Universität Leipzig, 118 pp. [Available from Institut für Meteorologie, Universität Liepzig, D-04103 Leipzig, Germany.]

——, and N. Mölders, 2000: On the influence of surface heterogeneity on latent heat-fluxes and stratus properties. *Atmos. Res.,* **54,** 59–85.

Groß, G., 1988: A numerical estimation of the deforestation effects on local climate in the area of the Frankfurt International Airport. *Contrib. Atmos. Phys.,* **61,** 219–231.

——, 1989: Numerical simulation of the nocturnal flow systems in the Freiburg area for different topographies. *Contrib. Atmos. Phys.,* **62,** 57–72.

Heymsfield, A. J., 1977: Precipitation development in stratiform ice clouds: A microphysical and dynamical study. *J. Atmos. Sci.,* **34,** 367–381.

——, and R. M. Sabin, 1989: Cirrus crystal nucleation by homogeneous freezing of solution droplets. *J. Atmos. Sci.,* **46,** 2252–2264.

Hinneburg, D., and G. Tetzlaff, 1996: Calculated wind climatology of the south-Saxonian/north-Czech mountain topography including an improved resolution of mountains. *Ann. Geophys.,* **14,** 767–772.

Jackson, D. A., K. M. Somers, and H. H. Harvey, 1989: Similarity coefficients: Measures of co-occurrence and association or simply measures of occurrence? *Amer. Nat.,* **133,** 436–453.

Kapitza, H., and D. P. Eppel, 1992: The non-hydrostatic mesoscale model GESIMA. Part I: Dynamical equations and tests. *Contrib. Phys. Atmos.,* **65,** 129–146.

Kramm, G., R. Dlugi, G. J. Dollard, T. Foken, N. Mölders, H. Müller, W. Seiler, and H. Sievering, 1995: On the dry deposition of ozone and reactive nitrogen compounds. *Atmos. Environ.,* **29,** 3209–3231.

Levkov, L., B. Rockel, H. Kapitza, and E. Raschke, 1992: 3D mesoscale numerical studies of cirrus and stratus clouds by their time and space evolution. *Contrib. Atmos. Phys.,* **65,** 35–58.

Loose, T., and R. D. Bornstein, 1977: Observations of mesoscale effects on frontal movement through an urban area. *Mon. Wea. Rev.,* **105,** 562–571.

Mölders, N., 1998: Landscape changes over a region in East Germany and their impact upon the processes of its atmospheric watercycle. *Meteor. Atmos. Phys.,* **68,** 79–98.

——, 1999a: On the atmospheric response to urbanization and open-pit mining under various geostrophic wind conditions. *Meteor. Atmos. Phys.,* **71,** 205–228.

——, 1999b: On the effects of different flooding stages of the Odra and different landuse types on the local distributions of evapotranspiration, cloudiness and rainfall in the Brandenburg–Polish border area. *Contrib. Atmos. Phys.,* **72,** 1–24.

——, 2000: Application of the principle of superposition to detect nonlinearity in the short-term atmospheric response to concurrent land-use changes associated with future landscapes. *Meteor. Atmos. Phys.,* **72,** 47–68.

——, A. Raabe, and G. Tetzlaff, 1996: A comparison of two strategies on land surface heterogeneity used in a mesoscale β meteorological model. *Tellus,* **48A,** 733–749.

——, G. Kramm, M. Laube, and A. Raabe, 1997a: On the influence of bulk-parameterization schemes of cloud microphysics on the predicted water-cycle relevant quantities—a case study. *Meteor. Z.,* **6,** 21–32.

——, U. Strasser, K. Schneider, W. Mauser, and A. Raabe, 1997b: A sensitivity study on the initialization of surface characteristics in meso-β/γ-modeling using digitized vs. satellite derived land-use data. *Contrib. Atmos. Phys.,* **70,** 173–187.

Ogunjemiyo, S., P. H. Schuepp, I. MacPherson, and R. L. Dejardins, 1997: Analysis of flux maps versus surface characteristics from Twin Otter grid flights in BOREAS 1994. *J. Geophys. Res.,* **102,** 29 135–29 145.

Olberg, M., and F. Rakóczi, 1984: *Informationstheorie in der Meteorologie und Geophysik.* Akademie Verlag, 181 pp.

Orlanski, I., 1976: A simple boundary condition for unbounded hyperbolic flows. *J. Comput. Phys.,* **21,** 251–269.

Pan, Z., E. Takle, M. Segal, and R. Arritt, 1999: Simulation of potential impacts of man-made land use changes on U.S. summer climate under various synoptic regimes. *J. Geophys. Res.,* **104,** 6515–6528.

Pielke, R. A., 1984: *Mesoscale Meteorological Modeling.* Academic Press, 612 pp.

——, G. Dalu, J. S. Snook, T. J. Lee, and T. G. F. Kittel, 1991: Nonlinear influence of mesoscale land use on weather and climate. *J. Climate,* **4,** 1053–1069.

——, R. L. Walko, L. T. Steyaert, P. L. Vidale, G. E. Liston, W. A. Lyons, and T. N. Chase, 1999: The influence of anthropogenic landscape changes on weather in south Florida. *Mon. Wea. Rev.,* **127,** 1663–1673.

Wilson, M. F., A. Henderson-Sellers, R. E. Dickinson, and P. J. Kennedy, 1987: Sensitivity of the Biosphere–Atmosphere Transfer Scheme (BATS) to the inclusion of variable soil characteristics. *J. Climate Appl. Meteor.,* **26,** 341–362.

WMO, 1971: Guide to meteorological instrument and observation practices. WMO Rep. 8 TP3, 151 pp.

Xue, Y., 1996: The impact of desertification in the Mongolian and the inner Mongolian grassland on the regional climate. *J. Climate,* **9,** 2173–2189.

Zhang, H., K. McGuffie, and A. Henderson-Sellers, 1996: Impacts of tropical deforestation. Part II: The role of large scale dynamics. *J. Climate,* **9,** 2498–2521.